robotics

MDPI

Article

HBS-1: A Modular Child-Size 3D Printed Humanoid

Lianjun Wu, Miles Larkin, Akshay Potnuru and Yonas Tadesse *

Received: 6 November 2015; Accepted: 4 January 2016; Published: 13 January 2016
Academic Editor: Huosheng Hu

Humanoid, Biorobotics and Smart Systems Laboratory (HBS Lab), Department of Mechanical Engineering, The University of Texas at Dallas, Richardson TX 75080, USA; lxw132630@utdallas.edu (L.W.); miles.larkin@gmail.com (M.L.); axp112630@utdallas.edu (A.P.)
* Correspondence: yonas.tadesse@utdallas.edu; Tel.: +1-972-883-4556; Fax: +1-972-883-4659

Abstract: An affordable, highly articulated, child-size humanoid robot could potentially be used for various purposes, widening the design space of humanoids for further study. Several findings indicated that normal children and children with autism interact well with humanoids. This paper presents a child-sized humanoid robot (HBS-1) intended primarily for children's education and rehabilitation. The design approach is based on the design for manufacturing (DFM) and the design for assembly (DFA) philosophies to realize the robot fully using additive manufacturing. Most parts of the robot are fabricated with acrylonitrile butadiene styrene (ABS) using rapid prototyping technology. Servomotors and shape memory alloy actuators are used as actuating mechanisms. The mechanical design, analysis and characterization of the robot are presented in both theoretical and experimental frameworks.

Keywords: humanoid; mechanical design; actuators; manufacturing; 3D printing

1. Introduction

Humanoid robots have great potential for use in our daily life by accompanying or working together with people. Growing interest in humanoid robots has spurred a substantial increase in their development over the past decade. Researchers have shown several prototypes in the literature focusing on various aspects. This paper primarily focuses on the design of a child-size humanoid robot named HBS-1. The overall form factor is an important parameter in the design of humanoids. As shown in Figure 1, a small humanoid robot that matches children 3–10 years old could be used for several application areas. These include teaching, training and therapeutic treatment for children with autism spectral disorder (ASD). The majority of children in this age range enjoy interacting with humanoids. The new idea presented in this paper is the design method of a humanoid, which is based on a combination of design for assembly (DFA) and design for manufacturing (DFM) for the full realization of humanoids in additive manufacturing. This paper tries to answer the fundamental question, such as how to design humanoid robots or what is the best approach to designing humanoids. The design requirements of the robot include: (1) being able to 3D print in an affordable 3D printer that can be housed in academic institutes; (2) being proportional to the actual size of a child in the age range of 6–12 years old; (3) being able to handle common objects of a load of 0.1kg in the hand; (4) having a sufficient degree of freedom in the upper body to manipulate objects; (5) using the design for assembly (DFA) and design for manufacturing (DFM) approaches; (6) being low cost in material; and (7) and serving as a platform to study artificial muscles. It is extremely important to review the existing humanoid robots in various categories and to describe their DOF, characteristics and cost to give a wider perspective to readers or researchers in the area. The existing humanoids can be categorized into three: humanoids with wheeled locomotion, humanoids with legged locomotion and humanlike robots [1].

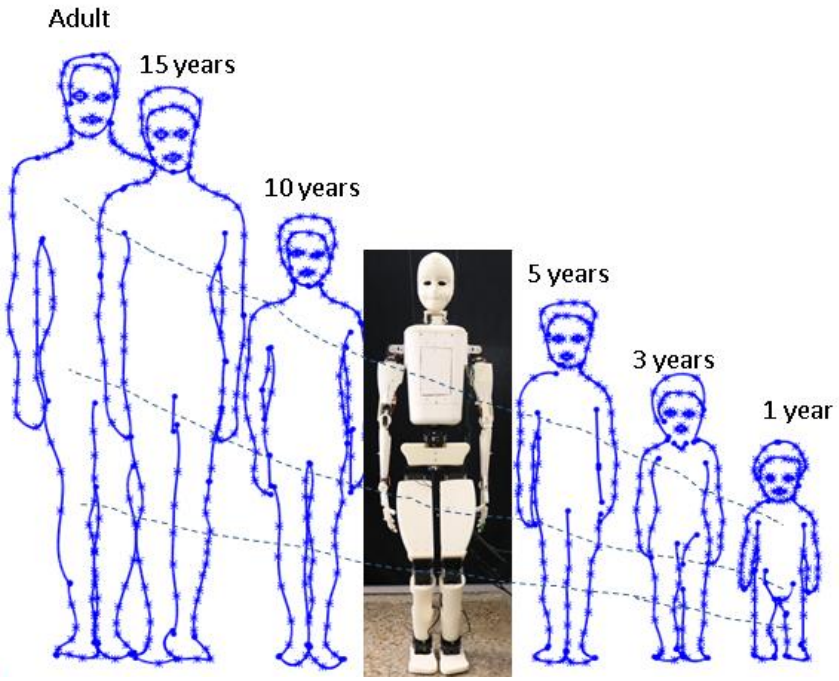

Figure 1. HBS-1 compared to humans (the schematic drawing is redrawn following the scale from Andrew Loomis [2]).

1.1. Humanoids with Legged Motion

Humanoids with legged motion are simply humanoid robots that have legs and can walk. Extensive research to improve the performance of bipedal robots has been conducted, from which many advanced and highly successful humanoids have emerged. In 1997, the design of a 35 DOF humanoid was presented for a fundamental research tool, model-based programming, vision research, for sensor integration and a testbed for adaptive behavior [3]. ASIMO (the most advanced humanoid) [4] is designed for useful roles in offices or households by interacting with humans through recognition of moving objects, postures and gestures. ASIMO is 130 cm tall, the size of an average nine-year-old boy, with 34 DOF, and costs around $1 million to buy and more than $100,000 to rent [5]. Robonaut 2 humanoid, designed by NASA and General Motors for use in space applications, can handle many tools, repair aircraft and communicate with astronauts in space [5]. It is 190 cm (6′3″) tall, costs about $2.5 million [5] and has 42 DOF. HRP-4C [6] is designed to work in human environments, uses tools like a human to manipulate objects and is able to speak and sing as an entertainment robot. It has 42 DOF, is the size of a 14-year-old adolescent, with 158 cm in height, and costs about $200,000 [7]. Mahru and Ahra [8] were developed to operate as network-based machines that can walk at a speed of 0.9 km/h (0.56 mph), talk and recognize gestures. They can both understand speech and learn from their own experience. They are 150 cm tall, the average 13-year-old boy, with a 35 DOF, and cost around $236,000 [9]. Pino [10] is developed by ZMP Inc. to accelerate the research and development of humanoids by providing technical information to the general public. It has a height of 70 cm, the average nine-month-old baby, 26 DOF, and costs around $30,000 [11]. Sony's QRIO [12] is designed to perform voice and face recognition; it can remember people's faces, as well as express its likes and dislikes. The costs of QRIO have been compared to the price of a luxury car [13]. It has 38 DOF and is 58 cm tall, about the size of a four-month-old baby. Toyota's Partner Robots [14] are being developed with human characteristics, which include being agile, friendly and intelligent enough to operate devices for personal assistance and care for the elderly. They are 83 cm tall, resembling a 1–6-year-old child. Kotaro [15] has a human-like skeletal structure and a flexible spine that acts very similar to human muscles. Kotaro is 133 cm tall, approximately the size of a nine-year-old child, with 91 DOF.

Poppy is a humanoid, which is also mostly 3D printed, like the humanoid presented in this paper. It is 84 cm tall, weighs 3 kg, has 25 motors and an LCD screen, and it costs around $11,000 [16,17].

1.2. Humanlike Robots

Humanlike robots are designed to mimic the appearance and behavior of humans realistically [1], such as facial movements (facial expressions). The robots may be legged, as in Albert HUBO [18] and HRP-4C [6], or stationary, as in SAYA [1] and Repliee Q2 [19]. Several examples are given in this section. EveR-4 [20] is an adult-sized entertainment robot that has a modular design for facial expressions and an artificial tongue. It is 180 cm tall and has 64 DOF. EveR-1, the first EveR model, costs $321,000 [21]. Zeno (RoboKind) [22] is designed by Hanson Robotics Inc. to behave and resemble a little boy. Zeno is 27-inches (67 cm) tall and has 37 DOF at a price of $ 16,750 [23]. Geminoid's HI-1 [19] is a life-sized humanlike robot that looks like its maker Hiroshi Ishiguro from Osaka University. While HI-1 lacks the ability to walk, it has a lifelike appearance and uses its 50 DOF to perform humanlike movements, including facial expressions. Repliee Q2 or Actroid [24] is a female humanlike robot that can do lifelike expressions, such as blinking, speaking and breathing. It has 42 DOF, 13 of which are in the head, and the rental cost is $3500 for five days [25]. A child size robot, iCUB (90 cm and <23 kg mass), was developed for cognitive study and is an open platform based on a 2.5-year-old child [26]. KASPAR is a minimally-expressive robot suitable for human-robot interaction studies, such as the treatment of autistic children. It is a low cost (around $2118 [27]) and effective product, as discussed in Dautenhahn *et al.* [28]. Roboy is another unique bio-inspired humanoid robot. It is designed based on musculoskeletal structures, which use tendon-driven actuation that provides soft and flexible motions. Its cost is around $270,000 [29,30]. There are many other humanoids presented in the literature and web resources, such as DARwln [31], CHARLI [32], Hanson Robokind [33], Nao [34], Nimbro-OP [35] and Kenshiro [36].

There are differences between "humanoids with legged motion" and "humanlike robots". For the former, the focus is on the mobility of the robot, whereas, in the latter, the focus is on the skin technology that makes the robot similar in appearance and behavior to humans. Some researchers combined legged motion with a humanlike appearance for the robot. One example is the Albert HUBO [18]. Albert HUBO robot is a legged robot and has 31 facial expressions.

1.3. Controllers Used in Humanoid Robots

Various processors are used in humanoid robots. The following are some examples from the literature. ASIMO uses five Pentium III Processor-M processors inside [37]. HRP-4C employs a PCI-104 single board computer and peripheral boards for the whole body motion control and distributed network motor drivers [6]. HUBO utilizes a laptop computer with wireless LAN [38]. DARwIn uses an onboard PC, 1.6-GHz Intel Atom Z530 with 4 GB SSD [32,39]. iCUB operates using DSP controllers, a PC104 relay station and a Pentium processor card [26]. CHARLI uses an Intel-based PC running GNU/Linux and a Robotis CM-730 sub-controller [32]. GNU is a Unix-like operating system. The processor's architecture in CHARLI is the same as DARwIn. CB uses the Arbor PC-104 Plus Em104P-i7013/PM1400 1.4-GHz Intel Pentium-M processor [34]. Mahru III [8] employs two CPU boards. QRIO [12] exploits three 64-bit MIPS processors [40]. NimbRo-OP [35] uses Zotac Zbox nano XS PC, Dual-Core AMD E-450 1.65 GHz and a Robotis CM730 board. POPPY [17] utilizes a TinyDuino processor board, Model ASM2001, consisting of an Atmel ATmega328P microcontroller.

For our humanoid HBS-1, we used a desktop computer (Intel i7(R) Core i7-4820k CPU@3.7 GHz with 16 GB RAM and a 64-bit operating system). The computer controls the robot while tethered, but we have purchased the PC-104 for future use for embedded computing and standalone operations. The PC-104 is widely used, and both the peripherals and input/output ports are sufficient for all intended applications.

1.4. Sensors Used in Humanoid Robots

Almost all humanoids use cameras for perception of the environment and object recognition. Additionally, force sensors are extensively used in various parts, either to interact with users or the environments. Touch sensors are used particularly in the hands, feet and torso. Another sensor is an inertial measurement unit (IMU), which includes an accelerometer, gyroscope and, sometimes, a magnetometer in one combined system. Audio sensory systems are employed for voice interactions. GPS and distance sensors (ultrasonic or laser based) facilitate navigation indoors and outdoors.

1.5. Comparison of Actuators Used in Humanoid Robots

Most humanoids employ electric motors. ASIMO utilizes a combination of brushless DC servomotors and harmonic drives [41]. HRP-4C uses electric motors [6]. HUBO employs a combination of a planetary gear and a harmonic gear with motors and belts or a pulley [38]. DARwIn and CHARLI exploit Dynamixel servos [32,39]. iCUB is based on a combination of a harmonic drive system (CSG series for major joints) and a brushless frameless motor (BLM) from Kollmorgen [26]. CB [34] uses hydraulic actuators [42]. Kenta and Kenshiro use MAXON brushless DC motors [36]. Mahru III [8] utilizes DC motors. QRIO [12,43] incorporates 38 motors. NimbRo-OP uses the Robotis Dynamixel MX series [35], and POPPY [17] requires 25 Robotis motors (MX-28).

The actuation technique is a prime design factor for researchers in humanoid design and development. The designs for a walking humanoid robot and lower limb orthosis that are actuated by pneumatic artificial muscles are documented in [44,45]. In general, electromagnetic-based actuators (electric motors) have greater than a 100-Hz bandwidth. If additional mechanical systems, such as gears, are incorporated along with the motors, the bandwidth will reduce almost by half (~50 Hz). Pneumatic and hydraulic actuators have limited bandwidth, usually below 10 Hz [46]. Among other actuators, dielectric elastomers are capable of a very high bandwidth (100–1400 Hz), while shape memory alloys work at a low bandwidth (<1 Hz) [47]. Concerning force or stress, shape memory alloy (SMA) is the highest energy density actuator, which can generate stress greater than 200 MPa. SMA wires of 25–510 μm in diameter are available commercially from Dynalloy Inc., Irvine, CA, USA; they can generate a force of 0.1–35 N. Pneumatic actuators, on the other hand, can provide high force (2500 N) [47]. The stress/force and bandwidth of the motors vary depending on the size of the motors. Nevertheless, the stress generated by these motors is much less than the SMA actuators. This is due to the large overall form factor of the actuation technology. A detailed discussion of numerous actuation technologies has been given in our prior works [47–50]. In all of the robots described above, actuators are extremely important to determine the performance of the robot, and care must be taken in selecting both the actuation systems and motion transmission accessories. Some additional design elements are strain rate, energy density (power/volume), specific power (power/weight), efficiency, electromechanical coupling, lifecycle, power consumption and sources, repeatability and response time. The maturity of the technology, ease of control and accessories demand further consideration. Detailed discussions are given in [47,48]

1.6. Goals of the Paper

This paper presents the design and manufacturing of a robot called HBS-1. The additive manufacturing technique is employed for the fabrication of the robot by using the 3D printer. The whole robot system is subdivided into several parts that can be independently created, modified, manufactured and replaced. Each part in the HBS-1 robot is designed in such a way that it can be easily 3D printed from acrylonitrile butadiene styrene (ABS) plastic using a 3D printer. The actuators (shape memory alloy for the hands and servomotors for all other joints) and mechatronic components are commercially available, which enables others to replicate the robot easily to perform further research. The overall material cost of the humanoid, including the mechanical and electrical system, is estimated to be ~$10,000. The cost can further be broken down into subcomponents. Actuators, including servos

and SMAs, cost $4923; the model and support materials (taking into account the rapid prototyping) cost $1662; and other mechatronic components (controllers, sensors, cameras) cost $2775. We aim to design a child-size robot that is cable of coexisting with humans, especially with children.

2. Design Approach of Humanoids

There are several approaches presented in the literature regarding humanoid design. These can be described as a bioinspired musculoskeletal design approach, the minimization of actuators approach, the concurrent design approach, the design for assembly and manufacturing, the modular design approach and the specific functionality approach. These are explained in the following paragraphs.

2.1. Bioinspired Musculoskeletal Design Approach

In this method, unique design approaches were presented based on musculoskeletal systems [31]. Some example robots designed with this approach are the Kenta (123 cm, 80 DOF), Kotaro (130 cm, 69 DOF), Kenzoh (135 cm, 58 DOF) and Kenshiro (90 cm, 46 DOF) robots. The authors of these robots have addressed the key question: how to design a complicated body structure and manage it. Similarly, a unique, cable-driven and highly compliant biologically-inspired robot design, the so-called ECCEROBOT, was presented in [51]. In another scenario, a neurobiological point of view of humanoid design was presented based on the flexible structure and their motor control units in [33], such as a 50 DOF humanoid called CB [34] and a 46 DOF ETL humanoid design [52].

2.2. Minimization of Actuators Approach

This case considers the minimization of the actuators, control and costs of the robots. Such robots fill the gap between the most complicated and the most simplistic ones. Some example robots are an 8 DOF humanoid [53], a humanoid with four actuators [54], a 16 DOF RoboNova [55], RE80II (24 DOF, 80 cm high, 7 kg weight) [56] and The Korea Advanced Institute of Science and Technology (KAIST) humanoid KHR-1 (12 DOF) [38]. These robots were designed based on low development cost, being lightweight, simple kinematics, high rigidity and uncertainty compensation.

2.3. Concurrent Engineering Approach

In a concurrent engineering approach, various teams work together to produce effective humanoid robots. Besides the multidisciplinary team involvement, a "role character" design process has been described by Oh *et al.* [57]. The concurrent engineering method requires multiple teams consisting of design engineers, manufacturing, mechatronics, sales and marketing, and many more. This is more suitable to large research institutes, centers or big companies that have huge investments.

2.4. Specific Functionality Approach

In this case, a particular robot function is the principal consideration in the design phase. One example is a humanoid with acrobatic motion capability (Morph3), as demonstrated in [58]. The robot used a tactile sensing shell in order to get pressure feedback for highly articulated motion. Furthermore, a jumping capability up to 4 cm in 110 ms required a unique rotatable joint, as discussed in [59]. HRP-2 walking patterns for dynamic stepping over a large obstacle are discussed in [60]. The HRP-2 main focus is on walking rather than mechanical design and overall system integration. In another study, the use of a psychological scale to evaluate the design of a humanoid based on a survey was described as a vital tool. The scale factors were familiarity, repulsion, performance, utility, motion, sound, voice and humanness [61].

2.5. Modular Behavior-Based Approach

This approach addresses the balance among hardware, software, mechanics, material and energy use, to design a better humanoid [62]. Recently, walking stabilization for a humanoid based on gait

analysis was studied. The relationship of foot landing, center of mass and leg stance was described in detail in [63]. Another proposal was an open platform DARwIn-OP based on a network-based modular structure and standard PC. The authors presented simulation software to study dynamic performance [50,64]. Other researchers proposed a design based on facial features in skeletal form. Two robots, BARTHOC and BARTHOC junior, were offered as a platform for multidisciplinary research in mechanical design [65]. More recently, the design of the facial expression for humanoids was proposed based on active drive points on the face of the robotic head [66].

2.6. Design for Assembly and Design for Manufacturing Approaches

The DFA method focuses mainly on the ease of assembling the robot in a short period. The key success of the NASA's Valkyrie robot is the ability to assemble its modules quickly. For a space mission, parts of the robot are packaged and assembled in space to reduce mission cost. DFM primarily considers the facilities at a firm or institute and attempts to fabricate the robot using available manufacturing methods.

In this paper, we considered both DFA and DFM principles to design HBS-1. The HBS-1 is not designed to rely on one actuation technology. Rather, it is intended to uses new actuators, such as coiled nylon that has been recently presented for finger actuation [67]. Therefore, the robot must be designed for ease in modification and assembly. The relation of additive manufacturing with DFM and DFA has been described in [68], where some of the guidelines (DFM and DFA) are not applicable for humanoid design directly. Therefore, since not all parts can be manufactured through rapid prototyping, custom-made designs were used to satisfy most of the guidelines. A summary of DFA and DFM approaches that were used for the design of HBS-1 are shown in Table 1 [69].

Table 1. Guidelines for the design of HBS-1 robot for design for manufacturing (DFM) and design for assembly (DFA).

Guidelines DFA	**Example**
Minimize the number of parts	HBS: the entire design.
Minimize the number of assembly operations	HBS: arms assembly (complex in shape).
Self-locating structures on part design	HBS: the entire torso design, pelvis and legs.
Modular design	HBS: each part can be made separately and assembled.
Part design symmetry	HBS: most parts.
Standardize parts and minimum use of fasteners	HBS: considering the manufacturing methods (8 × 8 × 11 in 3D printer), the number of fasteners was ~60.
Ease of part handling and insertion	HBS: all parts can be assembled without requiring special tools.
Guidelines DFM	**Example**
Ease of manufacturing(form, material and size)	HBS: almost 90% of the parts are 3D printed.
Use of standards parts	HBS: off the shelf fasteners, brackets and actuators.
Easily-made custom parts	HBS: the finger joints: metacarpophalangeal joints (MCP), proximal interphalangeal joints(PIP) and distal interphalangeal joint (DIP) used torsional springs made of music wire.
Capability of the manufacturing process	HBS: the gap between 3D printed moving parts was limited to 0.45 mm to minimize friction; the minimum feature size in a part is >3 mm; the minimum resolution of layer printing is 0.178 mm.
Part design symmetry	HBS: most parts.
Separate parts	HBS: considering the manufacturing methods (8 × 8 × 11 in 3D printer), two parts were made; for example, the torso.
Compliance	HBS: holes were chamfered, tapered and tolerance and a moderate radius were applied for the ease of insertion.

There are few papers that describe the design and manufacturing of humanoids. As noted earlier, Oh *et al.* showed the concurrent engineering approach as one solution [57]. However, such an approach is suitable to an institution with more manpower and may not be suitable for academic institutions with limited resources. Other than that, there is no clear explanation as to which design philosophies drive the humanoid robots' development. In our opinion, the most optimized approach would be that

of concurrent engineering, but due to the lack of availability of resources to satisfy its implementation, one can summarize that the preferred approach is ultimately dependent on the intended application of the robot.

3. Design and Fabrication

The HBS-1 is a new humanoid robot (Figure 2) that will be used as a platform for further research in humanoid robotics, educational and biomedical studies. Specific applications will be discussed further in Section 6.2. As highlighted in the Introduction section, the design requirements for HBS-1 were defined as follows: to build a child-sized robot with anatomically-correct dimensions that closely mimic human motion with sufficient DOF. The robot is to have the dimensions and features of a seven-year-old child and needs to be made entirely of 3D printed ABS parts and off the shelf components for maximum strength, simplicity and cost-effectiveness. Based on the DFM and DFA principles [70], all of the structural components (thigh, torso, forearm, *etc.*) are modular for ease of modification and maintenance. The number of parts is also minimized (DFA principle). The DOF, range of motion and torque of each joint should be sufficient, such that HBS-1 can sit, stand and perform articulated motion while stationary, as well as pick up and carry objects. It was desired to select all of the mechatronic components, including the microcontrollers, batteries, sensors and actuators, from commercially available products.

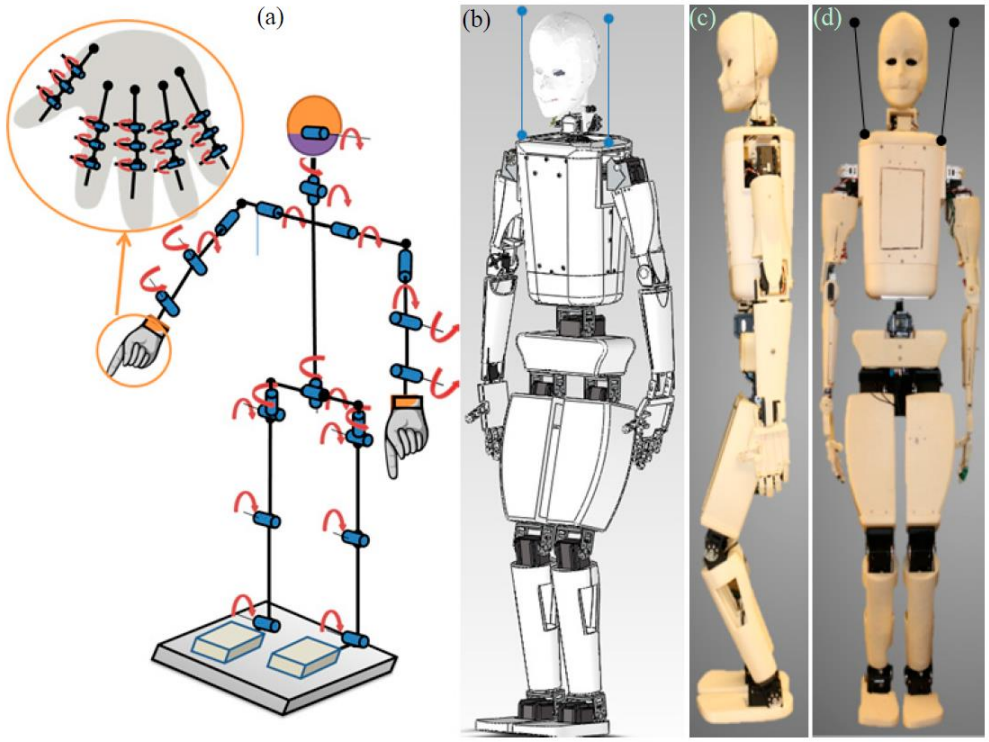

Figure 2. HBS-1: (**a**) Schematic layout; (**b**) CAD model; (**c**) Side view; (**d**) Front view of the prototype. The wires attached at the shoulder support the robot during testing.

3.1. Mechanical System

The overall dimension of robot HBS-1 is 120 cm × 33 cm × 14 cm in height, width and breadth, respectively, to match an average seven-year-old boy closely [71]. HBS-1 weighs ~5 kg and consists of two 4 DOF legs, a 2 DOF waist, two 4 DOF arms, two 15 DOF hands and a 3 DOF head (2 DOF neck + 1 DOF jaw), as seen in Figure 2. This gives HBS-1 a total of 51 DOF. The robot is powered by a DC power supply connected through wires while tethered. In the following section, the design of each part is described based on the design for manufacturing (DFM) and the design for assembling (DFA)

methods. These design principles are superimposed on the other considerations, such as cost, strength, architecture, autonomy and actuator performance. The design considerations and issues are common to many systems; a good example is found in hexapod robots in [72].

3.1.1. Head and Neck Design

The head/neck mechanism was designed to have 3 DOF: one for neck tilting, one for neck nodding and another for jaw movement. It was designed so that all parts are easily manufactured, modified, assembled or disassembled while looking and functioning as a human's head and neck. Previously, we have shown that a 2 DOF and linkage mechanism can effectively mimic the nodding and turning motion of the humanoid head [73]. The current head was divided into three parts, each having a thickness of 3 mm: the head, back cover and jaw. The 3D model of the head was generated from a 3D scan of a doll head and imported in SolidWorks™. The neck is made of two brackets for mounting the servos, as can be seen in Figure 3a, connecting the head to the body and allowing the head to pan and tilt.

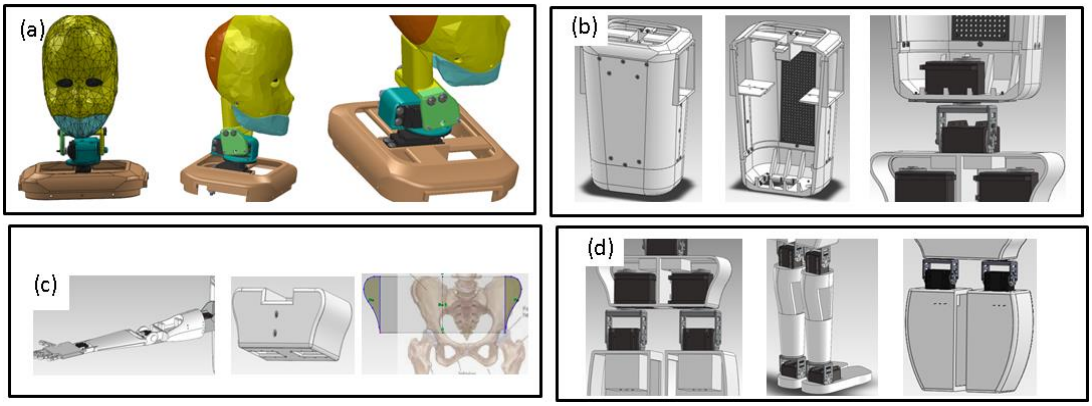

Figure 3. Design elements of HBS-1; (**a**) Head; (**b**) Exposed torso; (**c**) Arm, hand and pelvis; (**d**) Legs and feet.

3.1.2. Arm and Hand Design

The arm length of HBS-1 is 41 cm, matching the arm length of a seven-year-old boy [71]. Two servos are placed at the shoulder to mimic the human shoulder's ball joint, another at the elbow and at the wrist. The hand has five fingers, each with 3 DOF. The fingers are actuated by shape memory alloy (SMA) actuators, which are housed in the forearm. Torsional springs are installed at each finger joint for extension motion. The diameter of the SMAs is 130 µm (Dynalloy Inc., Irvine, CA, USA). According to the manufacturer, the 130-µm wires require 24 V/m and a current of I = 0.32 A. The maximum force of the actuator is 2.19 N, and the strain is 4%–5%. The hand design was presented at the ASME's International Mechanical Engineering Congress and Exposition(IMECE) conference in 2014 [74].

3.1.3. Torso Design

The torso, shown in Figure 3b, is 32.7 cm tall, 17.4 cm wide, 13.5 cm deep and has a wall thickness of 5 mm. It was designed to be 3D printed, house the majority of the electronics and have detachable sections for quick access to components mounted inside the torso. The 2 DOF waist consists of a roll and a pitch joint with the roll servo mounted at the bottom of the torso and the pitch servo mounted to the top of the pelvis. The maximum part size the printer can handle is 8″ × 8″ × 8″ (19.6 × 19.6 × 19.6 cm^3). With this in mind, the entire torso was split into four separate pieces for manufacturing: a front section, back section, top section and bottom section. Standoffs were added to the front and back sections of the torso to attach a solderless breadboard for mounting electronics.

3.1.4. Pelvis Design

The function of the pelvis is to house the thigh-roll servos, as can be seen in Figure 3c. To mimic the human form better, a picture of a human pelvis was used as a sketch picture for the sides of the pelvis, shown in Figure 3c. The back face of the pelvis was made into a detachable cover for access while mounting the thigh-roll servo. The assembled pelvis is 6 cm tall, 19 cm wide, 7.5 cm deep and has a wall thickness of 3 mm.

3.1.5. Leg Design

Each part of the legs was designed to be very strong while simple enough to allow for easy assembly and maintenance. The legs (4 DOF each) in Figure 3d are 53 cm long, and the shins and thighs have a wall thickness of 4 mm. The crotch length of HBS-1 is 58 cm, measured from the top of the thigh servo bracket to the floor, and its feet are 19 cm long and 7.5 cm wide, corresponding to a seven-year-old boy [71]. Most biped humanoid robots have 6 DOF in their legs; for example, HRP-4C [6], Mahru III [8], QRIO [12], NimbRo-OP [35] and HUBO [38]. However, iCUB [26] has 5 DOF, and other simple humanoids [53] have 2 DOF in their legs. Other humanoid designs based on musculoskeletal systems have 8 DOF in their legs, such as Kotaro [15]. In our robot, 4 DOF were chosen to minimize cost; the DOF are sufficient to perform the intended applications of our robot to interact with kids while standing in a frame structure or to perform articulated actions while tethered to the ground.

3.2. Fabrication

Except the mechatronic components, the HBS-1 was fabricated entirely by 3D printing using the Stratasys Dimension Elite 3D printer using ABS material. Acrylonitrile butadiene styrene (ABS) is a thermoplastic material with a yield strength of 31 MPa and a volume resistivity of 2.5×10^{15}–5.0×10^{16} Ω· cm [75]. There are several advantages in using 3D printers, such as the ability to create complex shapes and for reducing manufacturing time, cost and the amount of wasted material. In our case, manufacturing the humanoid's complex and intricate parts, such as the head, arms and fingers, would be very difficult without 3D printing. However, there are also several limitations of 3D printing using an FDM (fused deposition modeling) machine. One of the limiting features of the Stratasys Dimension Elite 3D printer is the size of the minimum printable feature, which is around 0.178 mm (0.007″), the size for the thickness of one layer of ABS plastic. This restricted the amount of detail in the model. The surface roughness of 3D printed parts also plays a significant role in moving parts, causing friction and restricting motion. In the 3D printing process, if there is not enough tolerance, the parts will fuse, rendering them useless. Several experiments were done to characterize the effect of the gap between moving parts. It was found that leaving a distance of 0.45 mm between moving parts would minimize the friction and allow the parts to move (for parts printed in assembly mode). Another disadvantage of the manufacturing process in the current 3D printers is that ABS plastic is significantly weakened when 3D printed. If those parts could be 3D printed with a much stronger material, the problem would be eliminated. Replacing the maximally-loaded thermoplastic ABS sections of HBS-1 with metal materials will maintain joint mobility and eliminate failures due to weak plastic. The relative magnitude of build materials and printing time of HBS-1 are shown in Figure 4. This figure shows the required model material, support materials (sacrificial materials that are dissolved by solvents after the parts are fabricated) and the required time of fabrication for each part of the robot. It can be seen that the total time of printing the robot is ~300 h. The figure is extremely important, since it tell us the necessary information in 3D printing humanoid robots depending on the size and the function of the robot. The 3D printer provides the exact amount of support and model materials when a CAD file is loaded to its operating software. Therefore, the magnitudes in Figure 4 are exact values without an error bar.

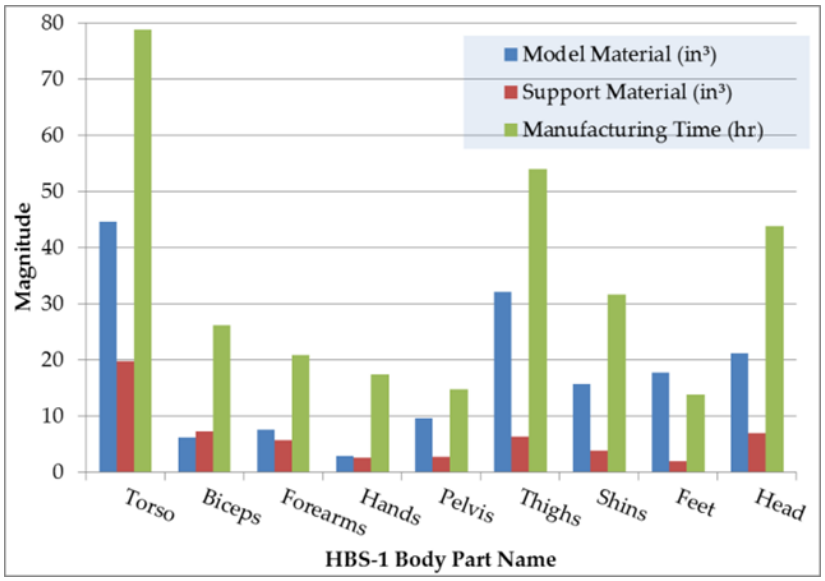

Figure 4. Manufacturing time, model material and support material for each part of HBS-1.

3.3. Mechatronic Systems

3.3.1. Actuators and Sensors for HBS-1

HBS-1 utilizes 14 Dynamixel servos, four Power HD servos and three Hitec Deluxe servos and shape memory alloy (SMA) actuators as its actuation system. Servo motor selection will be discussed further in Section 3.4. Dynamixel servos feature the ability to track the speed, temperature, shaft position and load in real time. Depending on the model, they can be controlled by Transistor-transistor logic (TTL), Serial communication (RS485) and controller area network (CAN) communication. The Dynamixel servos adopted were Models MX-106, MX-64 and RX-28. Dynamixel actuators are used in other robots [22,32,35], as well. Shape memory alloy actuators were selected in the current design, since they can be installed in the limited volume of the forearm. Otherwise, it would be difficult to actuate all five fingers.

Firewire stereo cameras are housed in the head. The torso is equipped with an orientation sensor (UM7-LT), which combines gyroscopes, accelerometers, magnetic sensors and an onboard 32-bit ARM Cortex processor to compute sensor orientation. The wires for the servomotors, as well as the shape memory alloy present some of the challenges of creating such robots. However, new sheath-core fibers and cables recently reported in [76] might be a promising solution for the robotic arms' or exoskeletons' wire connections. Since the mechatronic systems are obtained off the shelf, the use of multiple Dynamixel servos helps, since they can be easily daisy chained, making them easier to wire one another and reducing the time for wire assembly. This choice is in line with the DFA principles, which are presented in this paper. Moreover, 3D printable conductive thermoplastics are the other alternative to print directly on the 3D printed parts, as stated in [77], which would reduce the wiring requirements of the robot.

3.3.2. Controllers for HBS-1

Two servo controllers (Mini Maestro 24-Channel USB Servo and CM-700 Robotis) mounted within the torso were adopted for driving the 21 servomotors. The CM-700 Robotis Servo Controller, which communicates with the computer (Intel i7(R) Core (TM) i7-4820k CPU@3.7 GHz with 16 GB RAM and a 64-bit operating system) via the LN-101 USB Downloader, is responsible for the control of the Dynamixel servos. The Mini Maestro 24-Channel USB Servo Controller is used to control the Power HD servos and Hitec Deluxe servos. A custom-made controlling circuit, whose operating principles

and actuation sequences have been described by Tadesse *et al.* [50], was adapted to actuate the fingers using shape memory alloy actuators. The circuit is based on a PIC 8-bit microcontroller (16F874) that provides a sequence to H-bridge amplifiers (L298), whose outputs are connected to each SMA. The programing of the PIC microcontroller was done using the MPLAB IDE (Integrated Development Environment) board PICDEM™ 2 PLUS. Currently, the humanoid can be easily programmed through the microcontroller to perform a sequence of instructions to grasp an object in an open loop manner. The closed loop position control of the fingers using SMAs will be our future work.

3.3.3. Software and Programming of HBS-1

The servo controllers are programmed in Visual Studio using C++. For the implementation of the sequence of actuator movements, the controllers define the sequence using the robot motion controlling code. This enables the robot to have a uniform interface to communicate with two separate servo controllers. The sequence of the articulation of the robot while performing a particular task will be presented later in the section along with the video of the robot's motion. Some parts of the program that drives the Dynamixel servos are provided in the Appendix as an example. The entire code is long (~600 lines of code), since it has several cases that actuate various combinations of servos to perform different tasks.

3.4. Servo Motor Selection of HBS-1

As stated in the previous sections, HBS-1 is actuated using 21 servomotors. To choose adequate servos, the torque was determined at each joint with the robot in the pose that results in the maximum torque about that joint. The actual dynamics of the robot can be described as a function of joint variable q and its rate forms $\dot{q}$ and $\ddot{q}$ by the Lagrange equation [78]:

$$M(q)\ddot{q} + V_m\left(q, \dot{q}\right)\dot{q} + G(q) + F\left(\dot{q}\right) + \tau_d \;=\; \tau \tag{1}$$

where $M(q)$ is the inertia matrix, $V_m\left(q, \dot{q}\right)$ is the Coriolis/centripetal matrix, $G(q)$ is the gravitational component, $F\left(\dot{q}\right)$ is the friction component, τ_d is the unknown disturbances or unmodeled dynamics and τ is the torque at the joint. The robot has several revolute joints; hence, the dynamics was simplified by ignoring friction and Coriolis effects following the approach presented by Kanniah *et al.* (uncoupled links) [79]. The maximum torque that a servomotor has to overcome is a combination of static torque and dynamic torque. The total maximum torque can then be defined as:

$$T_{total} \;=\; \underbrace{\sum\left(M_i L_i\right)}_{Static} + \underbrace{\sum\left(I_{yyi}\alpha_i/g\right)}_{Dynamic} \tag{2}$$

where M_i is a force or weight acting on the moment arm at point i, L_i is the distance normal to the force, from i to the axis of rotation, I_{yy} is the mass moment of inertia about the axis of rotation, α is the desired angular acceleration of the arm and g is gravity.

3.4.1. Arms

The dimensions of the upper body used for calculating the static torque in the arms and torso joints are given in Table 2. Torque calculations for the wrist, elbow and shoulder servo motors were done with the torso leaning forward 30° and the arms parallel to the ground holding a 0.1-kg object straight out in front, as can be seen in Figure 5a. The moment of inertia I_{yy} for each joint was found using the parallel axis theorem, and the maximum angular acceleration was assumed to be 860 deg/s^2 (15 rad/s^2). Based on the results of these calculations, listed in Table 3, the arm servomotors were selected. The Power HD-1705MG Servo (0.196 N· m stall torque), the Power HD-6001HB Servo (0.657 N· m stall torque) and the Dynamixel RX-28 Robot Servo (2.744 N· m stall torque) were selected for the wrist, the elbow and the shoulder joints, respectively.

Table 2. Upper body dimensions for torque calculations (for Figure 5a).

Link (Object)	L_i (m)	W_i (N)	M_i (N)
Hand (block, i = 1)	0.105	0.196	0.98
Forearm (i = 2)	0.136	0.686	-
Bicep (i = 2)	0.146	1.47	-
Torso (i = 4)	0.119	16.366	9.8
Head (i = 5)	0.210	-	19.6

L_i = arm length, W_i = arm weight, M_i = load at the arm.

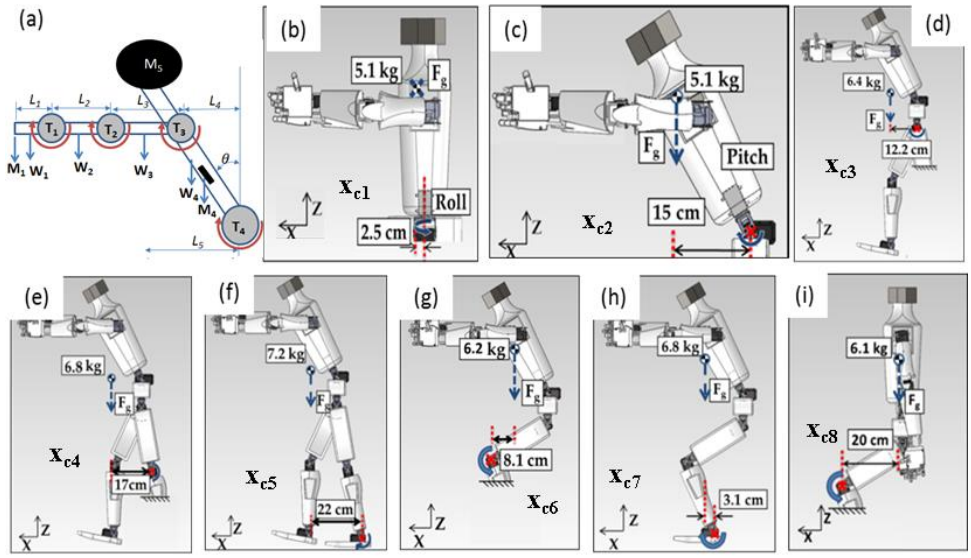

Figure 5. Various poses of the HBS-1 for torque calculation (**a**)–(**c**) arm and torso,(**d**)–(**i**) hip, knee and ankle.

3.4.2. Torso

The next two calculations are for the torso pitch and roll servos. As can be seen in Figure 5c, the torso pitch calculations were done with the robot holding a 0.1kg object and in the same position as the arm servo calculations, while the torso roll calculations were done with the torso in the upright position while holding a 0.1 kg object, shown in Figure 5b. The moment of inertia was found using the SolidWorks mass properties. The dynamic torques of the torso roll and pitch joints were then determined with an assumed maximum angular acceleration of 200 deg$\cdot$ s^{-2} (3.49 rad$\cdot$ s^{-2}), and the static torques were determined using the dimensions listed in Table 2. From the results listed in Table 3, the Dynamixel MX-106 with a stall torque of 10.388 N$\cdot$ m and the MX-64 with a stall torque of 6.272 N$\cdot$ m were chosen for the torso pitch servo and torso roll servo due to the compatibility with the MX-106 bracket, respectively.

Table 3. Upper body parameters and torque calculation results (for Figure 5a).

Joint	I_{yy}	α	T_s	T_d	T_i
	(kg$\cdot$ m^2)	(rad/s^2)	(N$\cdot$ m)	(N$\cdot$ m)	(N$\cdot$ m)
Wrist (i = 1)	2×10^{-3}	15	0.14	0.03	0.17
Elbow (i = 2)	0.01	15	0.32	0.17	0.49
Shoulder (i = 3)	0.03	15	0.90	0.45	1.37
Torso-pitch (i = 4)	0.47	3.5	7.25	1.67	8.82
Torso-roll (i = 5)	0.04	3.5	1.27	0.16	1.47

I_{yy} = moment of inertia about the y-axis, α = joint angular acceleration, T_s = static torque, T_d = dynamic torque, T_i = total torque.

3.4.3. Legs

The last servos to be selected were the hip/thigh, knee and ankle servos. Analyses were done for three different poses, shown in Figure 5d–i, on each of the three joints. Along with being able to find the moment of inertia, the mass properties tool in SolidWorks can also be used to approximate the static torque. The static torque equation can be simplified to:

$$T_s = x_c M_c \quad (3)$$

where x_c is the distance normal to gravity from the joint to the center of mass and M_c is the total mass acting on the body. The torso pitch and roll torques were recalculated using this method to verify its accuracy. The two methods (equivalent center of gravity and static component of Equation (2) correlate very well, with a <1 N· m difference between them. This center of gravity method was then used to determine the static torque for the thigh, knee and ankle servos, shown in Table 4.

Table 4. Parameters of the legs and torque determination (for Figure 5b–i).

Joint	x_{ci}	M_i	I_{yy}	α	T_s	T_d	T_i
	(m)	(N)	(kg· m^2)	(rad/s^2)		(N· m)	
T-Pitch (i = 2)	0.15	49.98	0.47	3.5	7.50	1.65	9.15
T-Roll (i = 1)	0.025	49.98	0.04	3.5	1.25	0.14	1.39
First Pose: Leaning forward, one leg on ground							
Thigh (i = 3)	0.12	62.72	0.9	1.6	7.52	1.44	8.96
Knee (i = 4)	0.17	66.64	2.1	1.6	11.33	3.36	14.69
Ankle (i = 5)	0.22	70.56	4.3	1.6	15.52	6.88	22.40
Second Pose: Squatting **							
Knee (i = 6)	0.081	60.76	1.2	1.6	4.92	1.92	6.84
Ankle (i = 7)	0.031	66.64	2.8	1.6	2.06	4.48	6.55
Third Pose: Sitting **							
Knee (i = 8)	0.20	59.78	1.5	1.6	11.96	2.4	14.36

** If the load is shared by both legs, the torque for each joint will be half the magnitude of the total. x_{ci} = distance to the center of mass, M_{ci} = center of mass at a pose.

The first pose (shown in Figure 5d–f) shows HBS-1 carrying a 0.1-kg object while leaning forward. As can be seen, the joint being calculated for is fixed, while the front leg is at the end of a step just before the front foot touches the ground. The second pose is HBS-1 squatting while holding the 0.1-kg object, shown in Figure 5g,h, and the third pose is HBS-1 at the end of a sitting motion with its arms reaching straight down, shown in Figure 5i. After analyzing each pose and using the variables in Table 4, the torques at the joints were determined. The MX-106 is the largest torque Dynamixel servomotor available on the market and is rated for 10.4 N· m, which is less than the maximum torque for the knee and ankle. Thus, the MX-106 was chosen for the thigh, knee and ankle servos. In this paper, since the dynamic walking is not analyzed, the operation of the robot can be maintained by limiting the maximum forward leaning angle. Furthermore, the feet are grounded to the floor, and two cords are attached to the shoulders and secured to a frame structure. Therefore, the current robot configuration is stable to perform various actions. Dynamic walking is beyond the scope of this paper and left for future work. Our focus in this paper is the upper body and the ability to perform articulated motion while the robot is tethered.

3.5. Shape Memory Alloy Selection for the Fingers

Due to the stringent requirement of a small space and a large force in the hands, low profile (small in size) and high energy density actuators are needed for the hands. SMAs can generate stress

to >200 MPa; their size is small (~100 µm diameter), and they provide strain up to 4% (cylindrical cross-section) and 200% (coiled forms). SMAs are available commercially in large quantities, and the operating frequencies of SMAs are less, 10 Hz (obtained by active cooling techniques), but in the range of human skeletal muscle frequency [49,80]. Further, these actuators are suitable for using a fuel-powered system, as demonstrated in [81]. The fuel cell systems have shown promise to power humanoid robots, as shown in [82]. SMAs have shown excellent results in humanoid development if the available space in the robot is a major concern; for instance, in the design of the head [50] and hands [74,83,84]. Therefore, SMAs are suitable candidates for finger actuation. Even though SMAs have hysteresis that makes them difficult to control, numerous papers have addressed the control challenges of SMAs. Some examples are a PID controller [85], a neural network [86], a multi-level switching controller [87], a nonlinear controller [88] and a neural network and sliding mode controllers [89].

4. Modeling and Analysis

4.1. Stress and Deformation Simulation

It is important to simulate the strength of the manufactured parts and to determine the capabilities. First, we have fabricated a cantilever beam of 100 × 10 × 1 mm in length, width and thickness and 3D printed (ABS material) with two printing options (normal and sparse high-density). The normal option fills the part completely with fully-dense raster tool paths, and the sparse high-density option minimizes the amount of model material, leaving some gaps in the interior regions. We then performed FEM simulation (static analysis) by loading the cantilever beam with a tip force corresponding 10-, 20-, 30- and 40 x 10^{-3} kg loads. SolidWorks™ 2014 was used for the simulation using the ABS material library. The model type was linear elastic isotropic. Static simulations were performed by setting the default meshing option. We then performed experiments on the fabricated cantilever beam (Figure 6a) with the same loads as in the simulation and determined the deflection using a camera. The experimental and simulation results of the deflection are close to each other, as shown in Figure 6b. The contour plots of displacement and the Von Mises stress of the cantilever beam are shown in Figure 6c,d, respectively. As the simulation and experimental results are comparable, one can conclude that similar properties will be shown on other 3D printed parts.

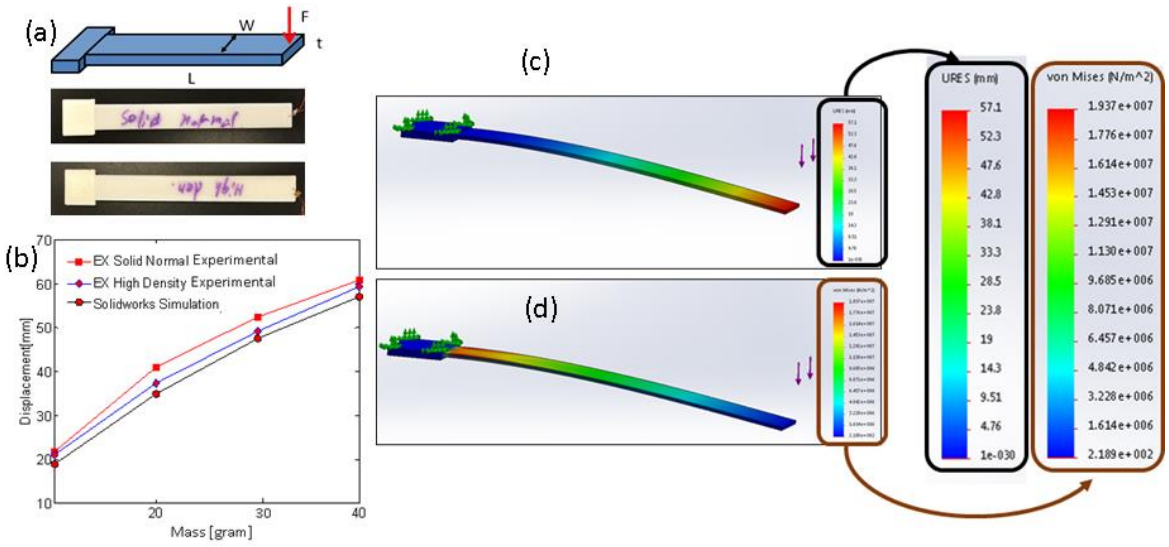

Figure 6. SolidWorks™ 2014 simulations of the displacement of a 3D printed cantilever beam (acrylonitrile butadiene styrene (ABS) material) loaded with a tip mass. (**a**) Schematic diagram and 3D printed cantilever with normal and sparse high-density printing options; (**b**) Displacement of the cantilever for tip mass load; experimental and simulation results; (**c**) Displacement contour plot simulation; and (**d**) Stress along the cantilever beam simulation at 40 × 10^{-3} kg tip load.

4.2. Stress Simulation of Robotic Finger

Since the fingers are the smallest parts of the 3D printed robot, we performed analysis on the fingers. First, we applied a 1-N force to various areas of the joints corresponding to the DIP, PIP and MCP joints. Metallic pin connectors (1 mm in diameter) were used at each joint, but all of the other parts were ABS material. Then, the deflection and stress were determined. It was found that the stress generated and displacement due to a 1-N load were 5.3 MPa and 0.18 mm (for an applied load at the tip of the DIP) observed on the ABS structures. The stress did not reach the maximum load carrying capacity of the ABS materials (31 MPa). Hence, the safety factor for carrying a 1-N load for the finger was about 5.8. The displacement and stress contour plots, as well as the loading conditions of the index finger, are shown in Figure 7a–c.

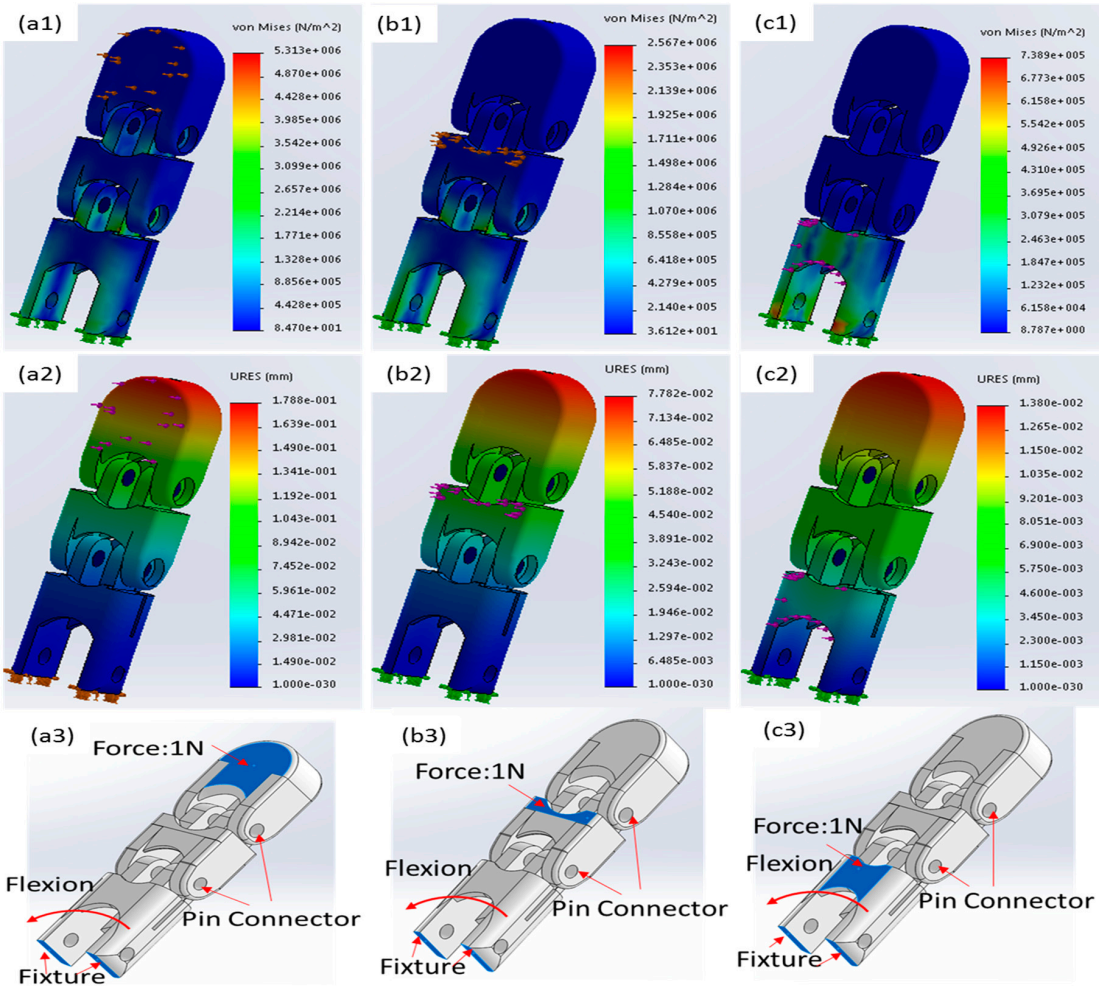

Figure 7. Simulations of the 3D printed index finger of ABS material with metallic pin connectors; loaded with a 1-N normal force. (**a**) On the DIP, (**b**) The PIP and (**c**) The MCP; the subscripts are: (**1**) For Von Mises stress in the finger; (**2**) Displacement in the finger; (**3**) Schematic diagram of the finger and boundary conditions.

Next, we made the entire robotic fingers with ABS material by making the pin connector with ABS material (1 mm in diameter) and performed stress simulations. It was found that when ABS pin connectors are used at the joints (as opposed to the metallic pin), the stress generated and displacement due to a 1-N load were 16.8 MPa and 0.12 mm (when the load is at the DIP section). The safety factor in this case was about two. The displacement, stress and loading conditions of the index finger results are shown in Figure 8a–c. The advantages of making the entire finger with 3D printable

materials include minimizing the assembly time and manual operations. However, the strength is somewhat compromised.

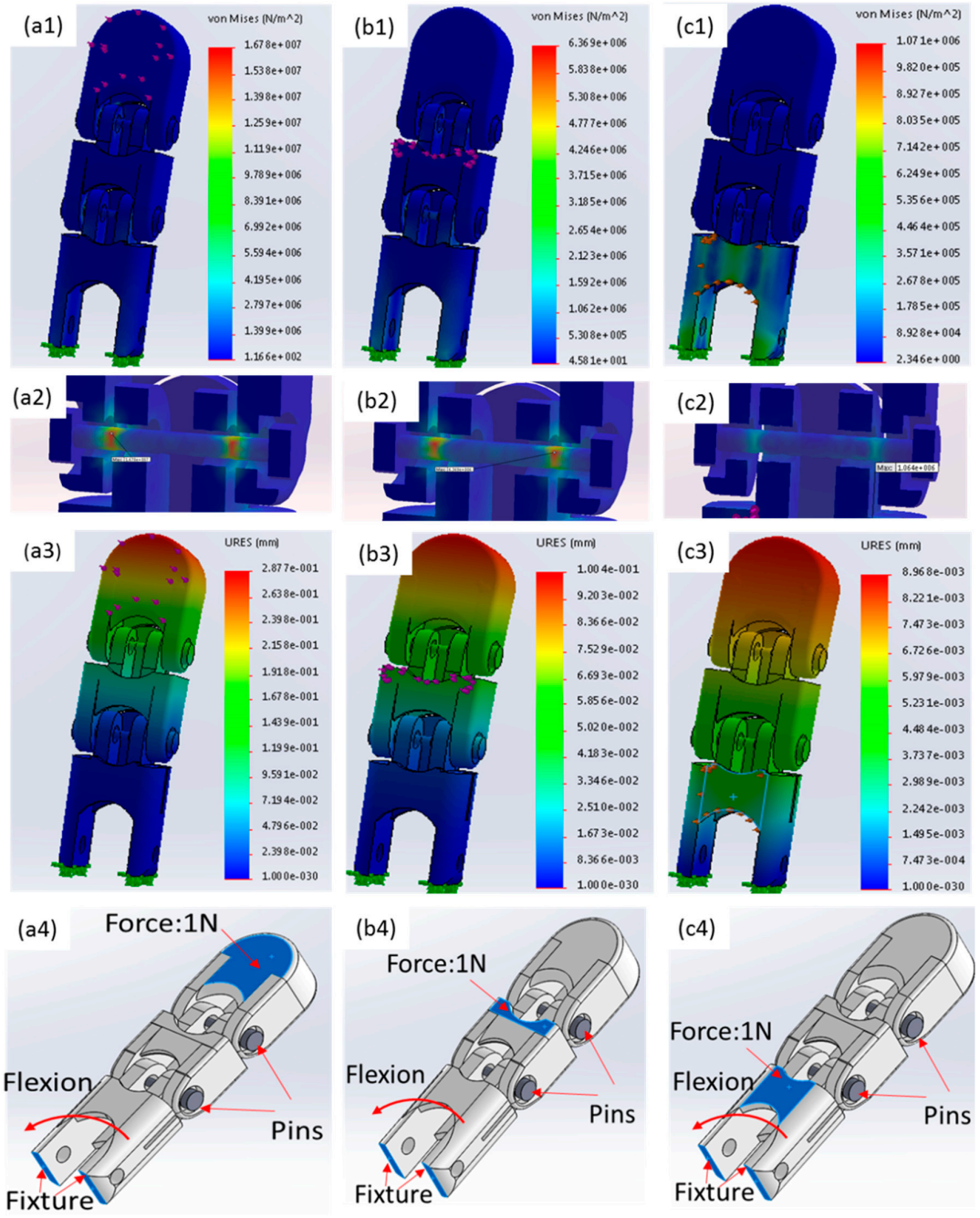

Figure 8. Simulations of index finger entirely 3D printed with ABS material (including the pins); loaded with a force of 1 N applied at: (**a**) The DIP, (**b**) The PIP and (**c**) The MCP. (**1**) Von Mises stress; (**2**) Magnified view of the Von Mises stress in the pin; (**3**) Displacement; and (**4**) Schematic diagram.

One concept of design for assembly (DFA) is to minimize the number of parts and fabricate entirely using a 3D printer. However, this notion is often challenged by the capabilities of the current manufacturing paradigm and the strength of the fabricated parts. Nevertheless, we proceeded to make the entire robotic finger with ABS material and to leave some gap (0.45 mm) between moving parts. The current design uses pins of 1 mm in diameter. As shown in Figure 8, we found that the cylindrical pin connectors made of ABS materials are susceptible to high stress for the intended load-carrying

capacity (1 N) depending on the geometry of the index finger under consideration. Further, if the pins were 3D printed, then they would be composed of around five layers of ABS plastic. This restricts the amount of detail that can be produced and affects the roundness of the pins. The challenges of such a manufacturing system will be overcome when new affordable 3D printers with composite materials and high resolution are made available on the market. In conclusion, the use of DFA will be extremely useful to advance humanoid research and bring robots to everyone in homecare for use in daily life.

4.3. DH Parameters and Workspace Analysis

In order to define the workspace for each arm of HBS-1, all of the possible end effector positions need to be found. This was done using the Denavit-Hartenberg convention [90]. The DH convention allows the position and orientation of the end effector to be represented in terms of rotations and translations related to the base coordinate system by using homogeneous transform matrices to transform a coordinate system from one joint of a robot arm to another. Each homogeneous joint transformation is represented as a product of four basic transformations: a rotation of angle θ around the current z-axis, a translation of distance d along the current z-axis, a translation of distance a along the new x-axis and, finally, a rotation of angle α around the new x-axis. The homogeneous joint transformation matrix $\boldsymbol{A_i}$ can be seen in Equation (4).

$$A_i = \begin{bmatrix} \cos(\theta_i) & -\cos(\alpha_i)\sin(\theta_i) & \sin(\alpha_i)\sin(\theta_i) & a_i\cos(\theta_i) \\ \sin(\theta_i) & \cos(\alpha_i)\cos(\theta_i) & -\sin(\alpha_i)\cos(\theta_i) & a_i\sin(\theta_i) \\ 0 & \sin(\alpha_i) & \cos(\alpha_i) & d_i \\ 0 & 0 & 0 & 1 \end{bmatrix} \tag{4}$$

$\boldsymbol{A_i}$ is a transformation matrix from one joint to another. Before determining the homogeneous transformation matrices, the origin and axes for each joint were selected. The DH parameters and axes for each joint are shown in Figure 9c. To make sure that HBS-1 was modeled correctly, we used MATLAB to compute and plot each joint and axis. From the MATLAB model and each joint transformation, we were able to find the location of the end effector with respect to the base frame. The workspace of HBS-1 was then plotted in MATLAB, as shown in Figure 9a. Inspection of Figure 9a shows that the arms can touch each other when they are located above the HBS-1's shoulders. The self-collisions of the robot arm can be avoided by controlling the joint angles through the visual C++ program that is used to actuate the robot. SolidWorks Macros were also used to display the workspace of one arm, so that a scale can be established relative to the robot, shown in Figure 9b. In conclusion, the DH simulation represents the workspace or the orientation capability of the humanoid without colliding with itself. This is one of the important parameters that shows the ability of the humanoid and can also be used to reverse engineer the humanoid joint variables for a particular application.

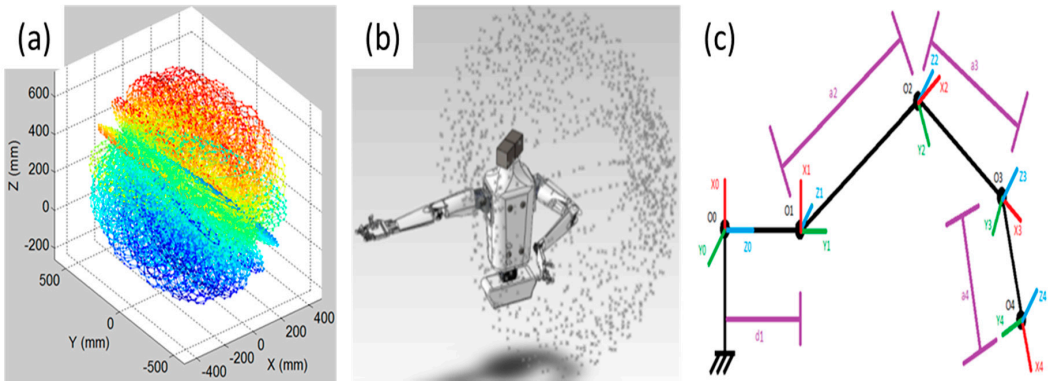

Figure 9. (**a**) 3D plot of the workspace of both arms; (**b**) Workspace of one arm with respect to the humanoid; (**c**) Schematic diagram of DH parameters.

5. Experiments

5.1. Angular Position and Speed of the Arm

To evaluate the arm servo performance, we performed the following experiments, from which the response time and the displacement of the servo were obtained. A black circular plate was attached to HBS-1's elbow for tracking with image processing software. A wooden ruler was placed in front of the arms to define the scale of the experiment. First, the HBS-1 arm was aligned in the horizontal direction as the initial position. Then, the arm's shoulder servo was actuated up and down while holding a load of 0.05 kg at the palm and without any load. The experimental video data were measured by recording the full movement of the arm and then performing further analysis on the video to obtain the response time. Both the total displacement and angular displacement of the tracked point on the right arm are shown in Figure 10. The arm starts moving at time 1.4 s. From Figure 10a, it can be seen that due to the extra load applied to the palm, the arm could not return to the original position. Figure 10b shows the angular position of the arm with and without a 0.05-kg load, and the difference is around five degrees.

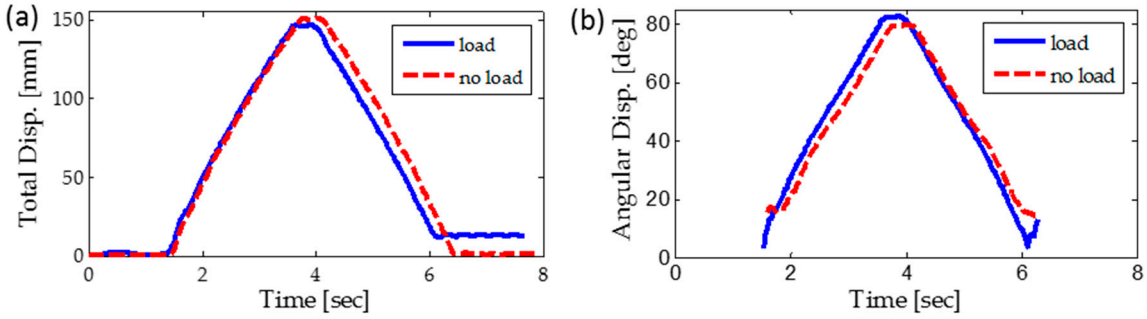

Figure 10. The displacement of tracking point on right arm: (**a**) Total displacement; (**b**) Angular displacement.

Other angular positions of the servo motors to mimic a child's game (similar to Patty Cake, popular among U.S. kids) are shown in Figure 11. The figure shows the sequence of the angles to perform an articulated motion sequence mimicking a game. The angles are symmetrical (the right and left shoulders in the X-direction) with respect to the direction of rotation and slight adjustments to magnitudes in the return motion (the right and left shoulder in the Z-direction) that assure collision-free motion of the robot hand. The waist (trunk X and Z) motion was actuated to mimic the gestures of the humanoid in performing gymnastic or child's games, as shown in Figure 11. A video of the actuation is provided as Supplementary Material (HBS_Action.MP4).

5.2. Grasping Capabilities

Small, humanlike prosthetic hand designs were taken into consideration when creating and evaluating the hand of HBS-1. The hand consists of five 3 DOF fingers. The challenge here is the limited space and the 4%–5% strain of SMA wires to drive the rotation of the finger joints, as described earlier. The wire (used as a tendon) is fixed at the end of the finger, while the SMA wire is attached to the other end of the wire, creating a pivoting moment about the joints. To achieve the needed linear displacement of the SMA wires, small pulleys with a wheel diameter of 6.35 mm were used. The arrangements of SMA on the hand can be seen in Figure 12a, and the hand grasping several objects is shown in Figure 12b–e. This test is a preliminary one that will be further explored infuture work.

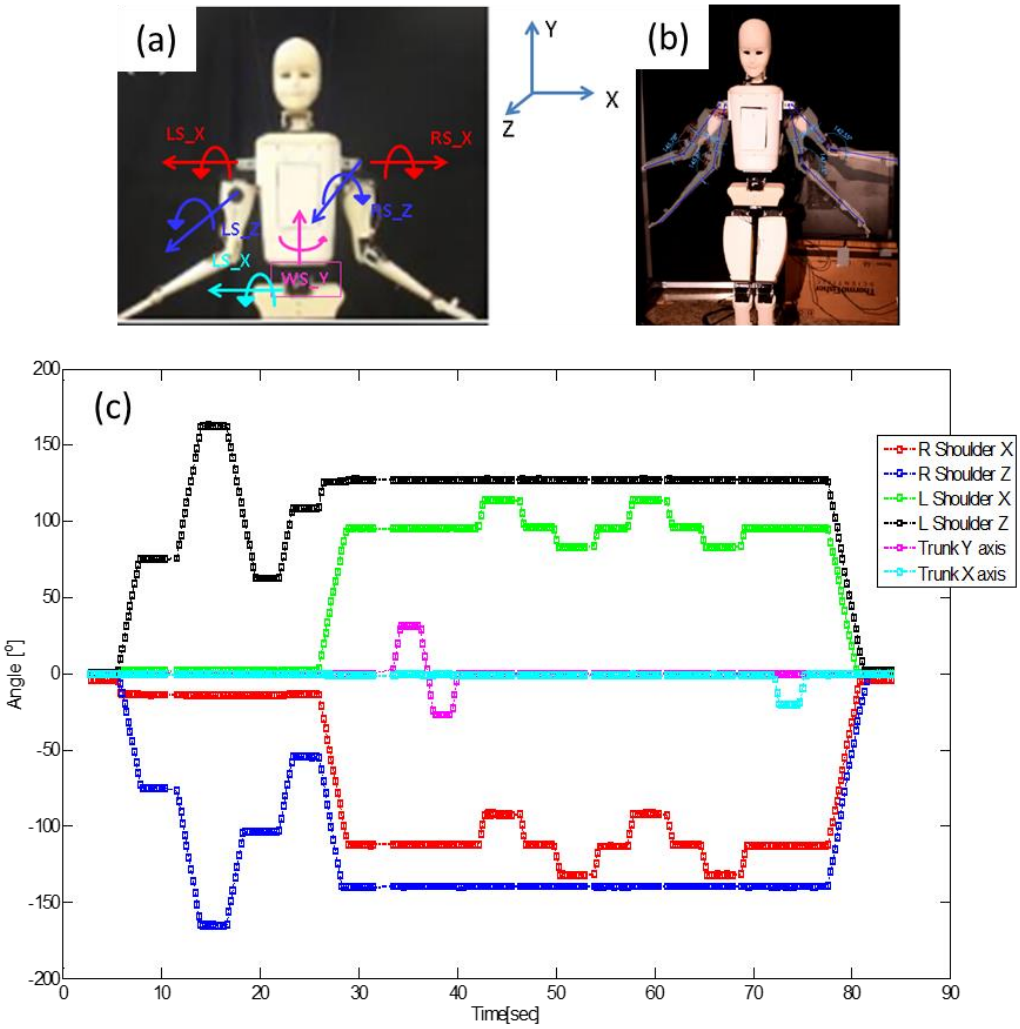

Figure 11. The sequence of motions of the servo motors of HBS-1 to mimic child games (**a**) servo arm axis representation (**b**) two sequence of motions overlaid and (**c**) time domain angular positions of the servos.

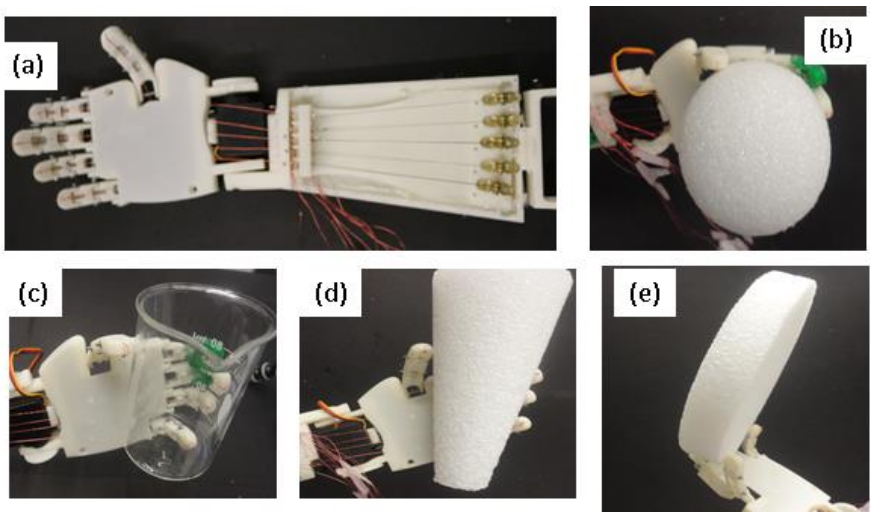

Figure 12. Shape memory alloy (SMA) hand. (**a**) Fingers actuated by SMA; and (**b**–**e**) The hand grasping various objects.

5.3. Various Poses

To observe the mobility and poses of the upper part of the HBS-1, a specific motion sequence was provided to each joint (the sequence shown in Figure 11c earlier). A video camera was used to record each pose, and the results are shown in snapshots in Figure 13. HBS-1's sequence of motion was planned so that it can interact with children safely and in an appealing manner. Figure 13a shows the arms at the initial position. Figure 13b,c shows the raised hand position from the horizontal. The full vertical extension of HBS-1 is shown in Figure 13d. Figure 13e,f shows a gymnastics gesture in which one arm is vertical and one arm is horizontal. Hugging gestures with (arms in front of its body) are shown in Figure 13g,h. Side to side twisting of the waist and rolling of hands over each other are shown from Figure 13h,p terminating in the robot's return to its original pose. Several videos were recorded to preserve its performance for further studies. The actuation video of HBS-1 is provided as a supplementary document in this paper (HBS_Action.MP4).

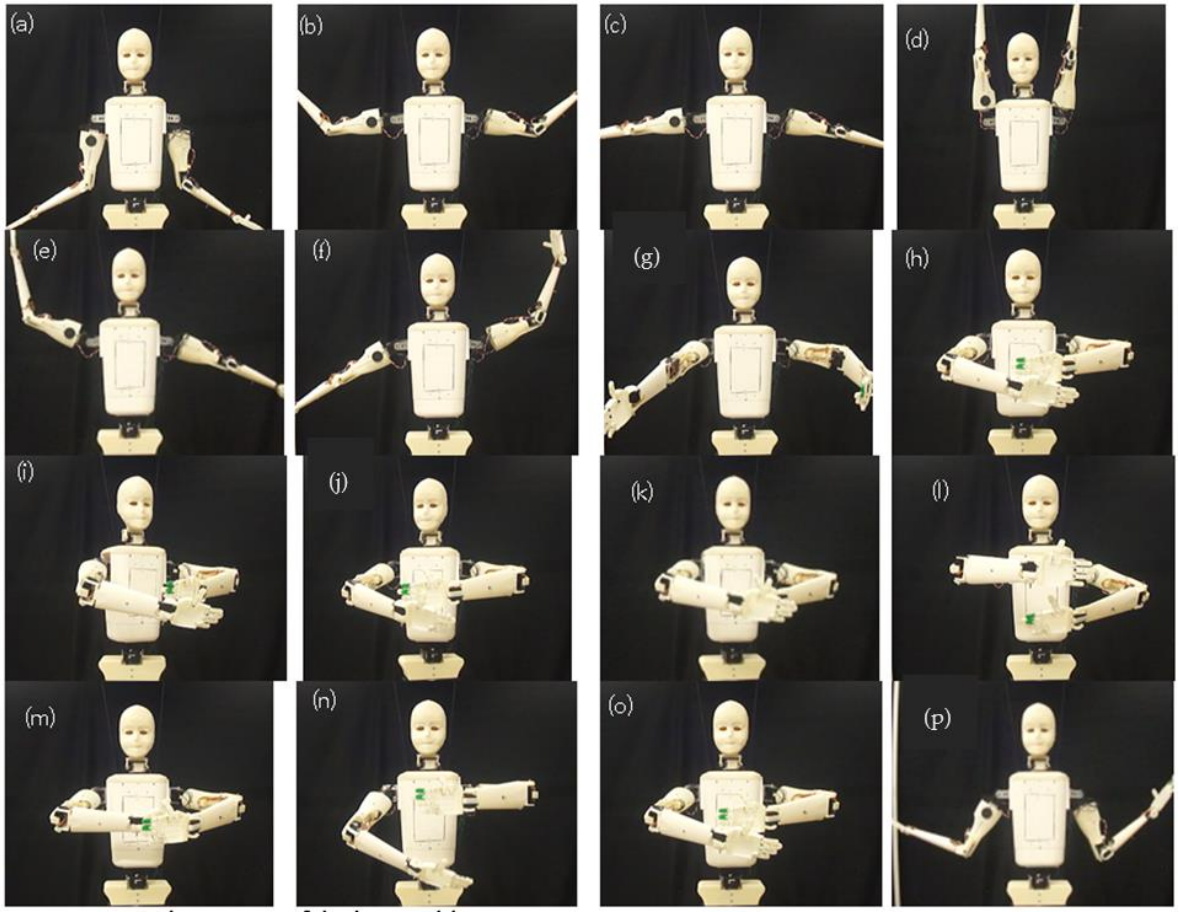

Figure 13. Various poses of the humanoid (**a**)–(**p**); sequentially actuated.

Currently, the HBS-1 robot is powered by a DC power supply (Topward Model 6306D). When all of the servomotors are actuated as shown in the video or the pictures in the characterization sections, the Dynamixel servos consume 14 V and 0.7 A. Similarly, the RC servomotors (Power HD Servos and Hitec Deluxe servos) consume 6 V and 0.6 A. The shape memory alloy (SMA) actuators used for actuation of fingers consume a voltage of 24 V/m and 0.32 A. The length of each SMA is about 240 mm, and we have five actuators in each hand. The power consumption for each SMA actuator is then 1.84 W. We can see that the total power consumption of the robot, when all actuators are simultaneously actuated, would be 31.8 W (ideal case). This is a high power requirement, but all actuators are not activated at the same time. The robot can be actuated with a Li-polymer battery, but the issue will be

the duration of the battery power. Therefore, further efforts are required to either reduce the power consumption or to get a higher power density rechargeable battery. These aspects will be investigated in the future.

6. Discussions and Applications

6.1. Discussion

The child-sized biped humanoid robot HBS-1 is a low-cost research platform for a wide range of robotics and related applications. It has a modular design and 51 DOF, designed for the ease of control and modification, and is made entirely of 3D printed parts and off the shelf components, which keeps the cost low while also having very anatomically-correct dimensions and features. Simulations and experiments were done to test its movement and grasping capabilities. The results showed that HBS-1 can closely mimic a human and can manipulate a variety of objects, shown in Figure 11, giving it the ability to perform a variety of tasks. In the future, several versions can be developed from HBS-1, each designed for specific applications. These possible applications are discussed in the following section.

6.2. Applications

There are four main areas of research and applications for HBS-1. The first is related to humanoid research: HBS-1 will be used to develop actuators and sensors that enable humanoids to more closely mimic humans using artificial muscles and artificial skin that senses touch, as well as manufacturing of humanoids and control theory. The second is education. HBS-1 in its current version would be an extremely useful teaching tool that can be used in university-level robotics courses. Its modular design allows for all types of sensors to be implemented, and its DOF (without considering the hands) makes control much simpler, both making HBS-1 excellent for use as an educational tool. Students would be able to learn the basics of robotics/humanoid control, modeling, manufacturing and design while working with a real humanoid. The third is medical. Future versions could be tailored to be used as a therapy tool for children with autism and other related disabilities. Research is currently being done using the HBS-1 to develop a muscle rehabilitation device that would otherwise be unsafe to test on a human first. The fourth is to use HBS-1 for a task that is difficult or dangerous for human beings. For example, handling and manipulating toxic or explosive substances. Since the robot is low cost, it can be made again (if it is destroyed during handling explosives) with the same architecture, design and manufacturing process.

The HBS-1 robot's modular design makes it very flexible, and it can be used in wide range of applications beyond the ones listed. Future works include integrating flesh-like elastomeric skin on the face and artificial muscles that actuate control points. Investigating a biped mountable robotic head following the approach presented in our earlier work [47,50], the robotic head that has 12 DOF in the face could be integrated with HBS-1 to create a very high degree of freedom humanoid robot. Moreover, a new approach that was demonstrated in [91] will be employed to design and analyze a facially-expressive robot, to integrate it with HBS-1 and, hence, to create a full humanoid with facial expression capability, for use in many application areas, such as healthcare [92].

7. Conclusions

We presented a low-cost, child-size, humanoid robot design, which was fabricated using 3D printing. The mechanical design of the humanoid, the modeling and stress simulations were performed to evaluate the design considerations to realize almost all of the structures using FDM, while maintaining the intended functionality of the robot and the anatomically correct child-size dimensions. The humanoid size is $120 \times 33 \times 14$ cm^3, and the total 3D printing time took 300 h. The overall material cost of the humanoid is ~$10,000. The workspace of its arms, determined using the DH method, is a $100 \times 120 \times 46$ cm^3 ellipsoid positioned at the midpoint between the left and right shoulder. The articulations of the joints enable the robot to demonstrate various children's games, which can further

be programmed to interact with children. The humanoid platform widens the design space of the existing humanoid intended for autism therapy, educational purpose or the general well-being of children through interactions. It can also be used for the research of artificial muscles to address most of the issues of control, the performance of artificial muscles and structural integrity concurrently. Shape memory alloy (SMA) was used to actuate the fingers of the humanoid, which are small and suitable for implementation. The hand can grasp and hold objects of various sizes and forms. The next step will be to partially cover the robot's parts with skin for safe human-robot interactions and to evaluate the effectiveness of the robot.

Acknowledgments: The authors would like to thank the support of the Mechanical Engineering Department (faculty start-up fund), Erik Jonsson School of Engineering and Computer Science, The University of Texas at Dallas. The authors would like to acknowledge: Alec Burns for DH modeling and analysis; Manoj Palanisamy for electronics and programming of the robot; Avinash Ramprakash and Peter-Michael Webb (summer intern) for some of the CAD designs; Poojan Khanpara for programming; Debalina Ghosh for the SMA circuit; and Richard S. Rome for editing the manuscript. Tadesse would like to acknowledge the support of the Office of Naval Research (ONR), Young Investigator Program.

Author Contributions: Lianjun Wu designed most of the robot, including the fabrication, characterization and stress simulations. Miles Larkin designed and analyzed the torso and legs during his MS studies. Akshay Potnuru performed the literature survey and contributed during the initial CAD model of the robot. Lianjun and Akshay performed the work as part of their Ph.D. studies, under the supervision of Yonas Tadesse. Tadesse directed the entire robot design and development from concept to application and manuscript preparation. All of the authors contributed to the technical writing and editing of the manuscript.

Conflicts of Interest: The authors declare no conflict of interest.

Appendix

Some examples of the code utilized for the HBS-1 robot actuation:

```
Dyn_eval(int *servPos)
{
    for(int i=0;i<NUM_DYN_SERVOS;i++)
    {
        if(i<2) continue; // Servos 0 and 1 are not present
        else if(*(servPos+i)<*(dynPosMin+i))
        {
            printf("Dynamixel Servo %d 's positions is less than the min position allowed for that servo!n",i);
            return FALSE;
        }
        else if(*(servPos+i)>*(dynPosMax+i))
        {
            printf("Dynamixel Servo %d 's positions is more than the max position allowed for that servo!n",i);
            return FALSE;
        }
        else continue;
    }
    return true;
}

void Dyn_moveTo(int *servPos)
{
    if(Dyn_eval(servPos))
    {
        for(int i=0;i<NUM_DYN_SERVOS;i++)
```

```
            {
                if(i<2) continue; // Servos 0 and 1 are not present
                if(servPos[i]==0)
                    continue; // Skips if the servo position is zero
                dxl_write_word( i, P_MOVING_SPEED_L, 56); // dxl_write_word( id, address, value);
                dxl_write_word( i, P_GOAL_POSITION_L, servPos[i]);
                int PresPos, CommStatus;
                PresPos = dxl_read_word( i, P_PRESENT_POSITION_L );
                CommStatus = dxl_get_result();
                if( CommStatus == COMM_RXSUCCESS )
                {
                    printf("The Current Pos of Dynamixel Servo %d is: %dn",i, PresPos);
                }
                else
                {
                    printf("Dynamixel Servo %d ERROR:",i);
                    PrintCommStatus(CommStatus);
                    printf("n");
                }
            }
            //Dyn_wait();
        }
        else printf("Position value entered exceeds the limit!n");
}

void Dyn_wait()
{
        int Moving;
        for(int i=0;i<NUM_DYN_SERVOS;i++)
        {
            if(i<2) continue; // Servos 0 and 1 are not present
            printf("%d",i);
            do
            {
                Moving = dxl_read_byte(i, P_MOVING );
                printf(">"); //std::this_thread::sleep_for(std::chrono::milliseconds(x));
            }while(Moving==1);
            printf("n");
        }
        return;
}
```

References

1. Bar-Cohen, Y.; Hanson, D.; Marom, A. *The Coming Robot Revolution*; Springer: Berlin, Germany; Heidelberg, Germany, 2009.
2. Loomis, A. *Figure Drawing for All It's Worth*; The Viking Press: New York, NY, USA, 1943.
3. Inaba, M.; Igarashi, T.; Kagami, S.; Inoue, H. Design and implementation of a 35 D.O.F. full-body humanoid that can sit, stand up and grasp an object. *Adv. Robot.* **1997**, *12*, 1–14. [CrossRef]

4. Sakagami, Y.; Watanabe, R.; Aoyama, C.; Matsunaga, S.; Higaki, N.; Fujimura, K. The intelligent asimo: System overview and integration. In Proceedings of the IEEE/RSJ International Conference on Intelligent Robots and Systems, Lausanne, Switzerland, 30 October–5 Novemver 2002; pp. 2478–2483.
5. Diftler, M.A.; Mehling, J.; Abdallah, M.E.; Radford, N.A.; Bridgwater, L.B.; Sanders, A.M.; Askew, R.S.; Linn, D.M.; Yamokoski, J.D.; Permenter, F. Robonaut 2—The First Humanoid Robot in Space. In Proceedings of the 2011 IEEE International Conference on Robotics and Automation (ICRA), Shanghai, China, 14 September 2011; pp. 2178–2183.
6. Kajita, S.; Kaneko, K.; Kaneiro, F.; Harada, K.; Morisawa, M.; Nakaoka, S.I.; Miura, K.; Fujiwara, K.; Neo, E.S.; Hara, I. Cybernetic human HRP-4c: A humanoid robot with human-like proportions. In *Robotics Research*; Springer: Berlin, Germany; Heidelberg, Germany, 2011; pp. 301–314.
7. Bridgwater, L.B.; Ihrke, C.; Diftler, M.A.; Abdallah, M.E.; Radford, N.A.; Rogers, J.; Yayathi, S.; Askew, R.S.; Linn, D.M. The robonaut 2 hand-designed to do work with tools. In Proceedings of the 2012 IEEE International Conference on Robotics and Automation (ICRA), Saint Paul, MN, USA, 14–18 May 2012; pp. 3425–3430.
8. Kwon, W.; Kim, H.K.; Park, J.K.; Roh, C.H.; Lee, J.; Park, J.; Kim, W.K.; Roh, K. Biped humanoid robot mahru III. In Proceedings of the 2007 7th IEEE-RAS International Conference on Humanoid Robots, Pittsburgh, PA, USA, 29 November–1 December 2007; pp. 583–588.
9. Robot Scientist Pushes Limits of Virtual Reality. Available online: http://www.koreaherald.com/view.php?ud= 20131225000122 (accessed on 30 July 2014).
10. Yamasaki, F.; Matsui, T.; Miyashita, T.; Kitano, H. Pino the humanoid: A basic architecture. In *Robocup 2000: Robot Soccer World Cup IV*; Springer: Berlin, Germany; Heidelberg, Germany, 2001; pp. 269–278.
11. Ambrose, R.O.; Savely, R.T.; Goza, S.M.; Strawser, P.; Diftler, M.A.; Spain, I.; Radford, N. Mobile manipulation using NASA's robonaut. In Proceedings of the IEEE International Conference on Robotics and Automation, New Orleans, LA, USA, 26 April–1 May 2004; pp. 2104–2109.
12. Endo, G.; Nakanishi, J.; Morimoto, J.; Cheng, G. Experimental studies of a neural oscillator for biped locomotion with qrio. In Proceedings of the IEEE International Conference on Robotics and Automation, Barcelona, Spain, 18–22 April 2005; pp. 596–602.
13. Rehnmark, F.; Ambrose, R.O.; Kennedy, B.; Diftler, M.; Mehling, J.; Bridgwater, L.; Radford, N.; Goza, S.M.; Culbert, C. Innovative robot archetypes for in-space construction and maintenance. In Proceedings of the Conference on Human/Robotic Technology and the National Vision for Space Exploration, Albuquerque, NM, USA, 13–17 February 2005.
14. Kubota, N.; Yorita, A. Structured learning for partner robots based on natural communication. In Proceedings of the IEEE Conference on Soft Computing in Industrial Applications, Muroran, Japan, 25–27 June 2008; pp. 303–308.
15. Mizuuchi, I.; Yoshikai, T.; Sodeyama, Y.; Nakanishi, Y.; Miyadera, A.; Yamamoto, T.; Niemela, T.; Hayashi, M.; Urata, J.; Namiki, Y. Development of musculoskeletal humanoid kotaro. In Proceedings of the IEEE Conference on Robotics and Automation, Orlando, FL, USA, 15–19 May 2006; pp. 82–87.
16. Davis, D.R.; Mehling, J.S.; Parsons, A.H.; Permenter, F.N.; Radford, N.A. Method and Apparatus for Electromagnetically Braking a Motor. Google Patents US8067909 B2, 29 November 2011.
17. Lapeyre, M.; Rouanet, P.; Oudeyer, P.Y. Poppy: A new bio-inspired humanoid robot platform for biped locomotion and physical human-robot interaction. In Proceedings of the 6th International Symposium on Adaptive Motion in Animals and Machines, Darmstadt, Germany, 11–14 March 2013.
18. Oh, J.H.; Hanson, D.; Kim, W.S.; Han, I.Y.; Kim, J.Y.; Park, I.W. Design of android type humanoid robot Albert HUBO. In Proceedings of the IEEE/RSJ International Conference on Intelligent Robots and Systems, Beijing, China, 9–15 October 2006; pp. 1428–1433.
19. Ishiguro, H.; Nishio, S. Building artificial humans to understand humans. *J. Artif. Organs* **2007**, *10*, 133–142. [CrossRef] [PubMed]
20. Ahn, H.S.; Lee, D.W.; Choi, D.; Lee, D.Y.; Hur, M.; Lee, H. Appropriate emotions for facial expressions of 33-DOFs android head ever-4 h33. In Proceedings of the IEEE International Workshop on RO-MAN, Paris, France, 9–13 September 2012; pp. 1115–1120.
21. Diftler, M.; Ahlstrom, T.; Ambrose, R.; Radford, N.; Joyce, C.; De La Pena, N.; Parsons, A.; Noblitt, A. Robonaut 2—Initial activities on-board the iss. In Proceedings of the IEEE Aerospace Conference, Big Sky, MT, USA, 3–10 March 2012; pp. 1–12.

22. Ranatunga, I.; Beltran, M.; Torres, N.A.; Bugnariu, N.; Patterson, R.M.; Garver, C.; Popa, D.O. Human-robot upper body gesture imitation analysis for autism spectrum disorders. In *Social Robotics*; Springer: Berlin, Germany; Heidelberg, Germany, 2013; pp. 218–228.
23. Davis, D.R.; Radford, N.A.; Permenter, F.N.; Valvo, M.C.; Askew, R.S. Integrated High-Speed Torque Control System for a Robotic Joint. Google Patents US8442684 B2, 14 May 2013.
24. Shimada, M.; Minato, T.; Itakura, S.; Ishiguro, H. Evaluation of android using unconscious recognition. In Proceedings of the 2006 6th IEEE-RAS International Conference on Humanoid Robots, Genova, Switzerland, 4–6 December 2006; pp. 157–162.
25. Davis, D.R.; Permenter, F.N.; Radford, N.A. System and Method for Calibrating a Rotary Absolute Position Sensor. Google Patents US8250901 B2, 28 August 2012.
26. Tsagarakis, N.G.; Metta, G.; Sandini, G.; Vernon, D.; Beira, R.; Becchi, F.; Righetti, L.; Santos-Victor, J.; Ijspeert, A.J.; Carrozza, M.C.; *et al*. Icub: The design and realization of an open humanoid platform for cognitive and neuroscience research. *Adv. Robot.* **2007**, *21*, 1151–1175. [CrossRef]
27. Tsai, M.J.; Wu, C.T. Study of mandible reconstruction using a fibula flap with application of additive manufacturing technology. *BioMed. Eng. Online* **2014**, *13*, 57. [CrossRef] [PubMed]
28. Dautenhahn, K.; Nehaniv, C.L.; Walters, M.L.; Robins, B.; Kose-Bagci, H.; Mirza, N.A.; Blow, M. Kaspar—A minimally expressive humanoid robot for human-robot interaction research. *Appl. Bionics Biomech.* **2009**, *6*, 369–397. [CrossRef]
29. Kumar, P.K.; Lagoudas, D.C.; Zanca, K.J.; Lagoudas, M.Z. Thermomechanical characterization of high temperature sma actuators. In Proceedings of the International Society for Optics and Photonics, Smart Structures and Materials, San Diego, CA, USA, 26 Feburary 2006; pp. 12–17.
30. Pfeifer, R.; Iida, F.; Lungarella, M. Cognition from the bottom up: On biological inspiration, body morphology, and soft materials. *Trends Cognit. Sci.* **2014**, *18*, 404–413. [CrossRef] [PubMed]
31. Nakanishi, Y.; Ohta, S.; Shirai, T.; Asano, Y.; Kozuki, T.; Kakehashi, Y.; Mizoguchi, H.; Kurotobi, T.; Motegi, Y.; Sasabuchi, K. Design approach of biologically-inspired musculoskeletal humanoids. *Int. J. Adv. Robot. Syst.* **2013**, *10*. [CrossRef]
32. Lee, D.D.; Yi, S.J.; McGill, S.; Zhang, Y.; Behnke, S.; Missura, M.; Schulz, H.; Hong, D.; Han, J.; Hopkins, M. Robocup 2011 humanoid league winners. In *Robocup 2011: Robot Soccer World Cup XV*; Springer: Berlin, Germany; Heidelberg, Germany, 2012; pp. 37–50.
33. Giszter, S.F.; Moxon, K.A.; Rybak, I.; Chapin, J.K. A neurobiological perspective on humanoid robot design. *IEEE Intell. Syst.* **2000**, *15*, 64–69. [CrossRef]
34. Cheng, G.; Hyon, S.H.; Morimoto, J.; Ude, A.; Hale, J.G.; Colvin, G.; Scroggin, W.; Jacobsen, S.C. Cb: A humanoid research platform for exploring neuroscience. *Adv. Robot.* **2007**, *21*, 1097–1114. [CrossRef]
35. Schwarz, M.; Pastrana, J.; Allgeuer, P.; Schreiber, M.; Schueller, S.; Missura, M.; Behnke, S. Humanoid teensize open platform nimbro-op. In Proceedings of the 17th RoboCup International Symposium, Eindhoven, The Netherlands, 30 June 2013.
36. Kozuki, T.; Motegi, Y.; Shirai, T.; Asano, Y.; Urata, J.; Nakanishi, Y.; Okada, K.; Inaba, M. Design of upper limb by adhesion of muscles and bones—Detail human mimetic musculoskeletal humanoid kenshiro. In Proceedings of the IEEE/RSJ International Conference on Intelligent Robots and Systems, Tokyo, Japan, 3–7 November 2013; pp. 935–940.
37. Byko, M. Personification: The Materials Science and Engineering of Humanoid Robots. Available online: http://www.tms.org/pubs/journals/JOM/0311/Byko-0311.html (accessed on 20 October 2015).
38. Park, I.W.; Kim, J.Y.; Lee, J.; Oh, J.H. Mechanical design of the humanoid robot platform, HUBO. *Adv. Robot.* **2007**, *21*, 1305–1322. [CrossRef]
39. Robotis. Available online: http://www.robotis.com/xe/ (accessed on 7 April 2014).
40. Hara, Y. Sony's Qrio Robot Hits the Ground Running. Available online: http://www.eetimes.com/document.asp?doc_id= 1147759 (accessed on 20 October 2015).
41. Asimo Technical Information. Available online: http://asimo.honda.com/downloads/pdf/asimo-technical-information.pdf (accessed on 20 October 2015).
42. Legged Locomotion. Available online: http://www-clmc.usc.edu/Research/LeggedLocomotion (accessed on 20 October 2015).

43. Geppert, L. Qrio: The Robot That Could. Available online: http://spectrum.ieee.org/robotics/robotics-software/qrio-the-robot-that-could (accessed on 20 October 2015).
44. Narioka, K.; Hosoda, K. Designing synergistic walking of a whole-body humanoid driven by pneumatic artificial muscles: An empirical study. *Adv. Robot.* **2008**, *22*, 1107–1123. [CrossRef]
45. Dzahir, M.A.M.; Yamamoto, S.I. Recent trends in lower-limb robotic rehabilitation orthosis: Control scheme and strategy for pneumatic muscle actuated gait trainers. *Robotics* **2014**, *3*, 120–148. [CrossRef]
46. Van Ninhuijs, B.; van der Heide, L.; Jansen, J.; Gysen, B.; van der Pijl, D.; Lomonova, E. Overview of actuated arm support systems and their applications. *Actuators* **2013**, *2*, 86–110. [CrossRef]
47. Tadesse, Y. Actuation technologies for humanoid robots with facial expressions (hrwfe). *Trans. Control Mech. Syst.* **2013**, *2*, 1–10.
48. Tadesse, Y. Actuation technologies suitable for humanoid robots. In Proceedings of the ASME 2012 International Mechanical Engineering Congress and Exposition, Houston, TX, USA, 9–15 November 2012; American Society of Mechanical Engineers: New York, NY, USA, 2012; pp. 1–10.
49. Tadesse, Y. Electroactive polymer and shape memory alloy actuators in biomimetics and humanoids. In Proceedings of the SPIE Smart Structures and Materials+ Nondestructive Evaluation and Health Monitoring, San Diego, CA, USA, 12–13 March 2013; pp. 9–12.
50. Tadesse, Y.; Hong, D.; Priya, S. Twelve degree of freedom baby humanoid head using shape memory alloy actuators. *J. Mech. Robot.* **2011**, *3*, 011008. [CrossRef]
51. Jovanovic, K.; Potkonjak, V.; Holland, O. Dynamic modeling of an anthropomimetic robot in contact tasks. *Adv. Robot.* **2014**, *28*, 793–806.
52. Nagakubo, A.; Kuniyoshi, Y.; Cheng, G. The etl-humanoid system—A high-performance full-body humanoid system for versatile real-world interaction. *Adv. Robot.* **2003**, *17*, 149–164. [CrossRef]
53. Hari Krishnan, R.; Vallikannu, A. A semi-minimalistic approach to humanoid design. *Int. J. Sci. Res. Publ.* **2012**, *2*, 1–6.
54. Shome, S.N.; Basu, J.; Sinha, G.P. *Proceedings of the National Conference on Advanced Manufacturing & Robotics*; Allied Publishers: New Delhi, India, 2004.
55. Grunberg, D.; Ellenberg, R.; Kim, Y.; Oh, P. From Robonova to HUBO: Platforms for robot dance. In *Progress in Robotics*; Kim, J.H., Ge, S., Vadakkepat, P., Jesse, N., al Manum, A., Puthusserypady, K.S., Rückert, U., Sitte, J., Witkowski, U., Nakatsu, R., *et al*, Eds.; Springer: Berlin, Germany; Heidelberg, Germany, 2009; Volume 44, pp. 19–24.
56. Zhou, C.; Yue, P.K. Robo-erectus: A low-cost autonomous humanoid soccer robot. *Adv. Robot.* **2004**, *18*, 717–720. [CrossRef]
57. Oh, K.; Kim, J.; Kim, M. Development of humanoid robot design process-focused on the concurrent engineering based humanoid robot design. In Proceedings of the IASDR Conference, Yunlin, Taiwan, 11–14 November 2005.
58. Okumura, Y.; Tawara, T.; Furuta, T.; Endo, K.; Shimizu, M.; Shimomura, M.; Kitano, H. Morph3: A compact-size humanoid robot system capable of acrobatic behavior. *Adv. Robot.* **2004**, *18*, 699–710. [CrossRef]
59. Zhu, C.; Kawamura, A. Development of biped robot mari-3 for jumping. *Adv. Robot.* **2010**, *24*, 1661–1675. [CrossRef]
60. Stasse, O.; Verrelst, B.; Wieber, P.B.; Vanderborght, B.; Evrard, P.; Kheddar, A.; Yokoi, K. Modular architecture for humanoid walking pattern prototyping and experiments. *Adv. Robot.* **2008**, *22*, 589–611. [CrossRef]
61. Kamide, H.; Kawabe, K.; Shigemi, S.; Arai, T. Development of a psychological scale for general impressions of humanoid. *Adv. Robot.* **2013**, *27*, 3–17. [CrossRef]
62. Lund, H.H.; Pagliarini, L. Modular behavior-based control for team humanoids. *Adv. Robot.* **2004**, *18*, 659–676. [CrossRef]
63. Hashimoto, K.; Takezaki, Y.; Lim, H.O.; Takanishi, A. Walking stabilization based on gait analysis for biped humanoid robot. *Adv. Robot.* **2013**, *27*, 541–551. [CrossRef]
64. Ha, I.; Tamura, Y.; Asama, H. Development of open platform humanoid robot darwin-op. *Adv. Robot.* **2013**, *27*, 223–232. [CrossRef]
65. Hackel, M.; Schwope, S.; Fritsch, J.; Wrede, B.; Sagerer, G. Designing a sociable humanoid robot for interdisciplinary research. *Adv. Robot.* **2006**, *20*, 1219–1235. [CrossRef]

66. Yu, Z.; Ma, G.; Huang, Q. Modeling and design of a humanoid robotic face based on an active drive points model. *Adv. Robot.* **2014**, *28*, 379–388. [CrossRef]
67. Wu, L.; Jung de Andrade, M.; Rome, R.S.; Baughman, R.H.; Tadesse, Y. Nylon-muscle-actuated robotic finger. In Proceedings of the SPIE Biological-Inspired Systems and Bio-MEMS, San Digeo, CA, USA, 2 April 2015.
68. Gibson, I.; Rosen, D.W.; Stucker, B. *Additive Manufacturing Technologies: Rapid Prototyping to Direct Digital Manufacturing*; Springer: Berlin, Germany; Heidelberg, Germany, 2009.
69. Boothroyd, G.; Dewhurst, P.; Knight, W.A. *Product Design for Manufacture and Assembly*, 3rd ed.; Taylor & Francis: Boca Raton, FL, USA, 2010.
70. Ulrich, K.T.; Eppinger, S.D. *Product Design and Development*; McGraw-Hill: New York, NY, USA, 2012.
71. Snyder, R.G.; Spencer, M.L.; Owings, C.L.; Schneider, L.W. Anthropometry of US Infants and Children. *SAE Tech. Pap.* **1975**, 750423. [CrossRef]
72. Tedeschi, F.; Carbone, G. Design issues for hexapod walking robots. *Robotics* **2014**, *3*, 181–206. [CrossRef]
73. Tadesse, Y.; Subbarao, K.; Priya, S. Realizing a humanoid neck with serial chain four-bar mechanism. *J. Intell. Mater. Syst. Struct.* **2010**, *21*, 1169–1191. [CrossRef]
74. Wu, L.; Tadesse, Y. Humanoid robot hand with sma actuators and servo motors. In Proceedings of the ASME 2014 International Mechanical Engineering Congress and Exposition, Montreal, QC, Canada, 14–20 November 2014; American Society of Mechanical Engineers: New York, NY, USA, 2014.
75. Abs Plus-p430, Production-Grade Thermoplastic for Design Series 3d Printers. Available online: http://usglobalimages.stratasys.com/Main/Files/Material_Spec_Sheets/MSS_FDM_ABSplusP430.pdf (accessed on 4 November 2015).
76. Liu, Z.; Fang, S.; Moura, F.; Ding, J.; Jiang, N.; Di, J.; Zhang, M.; Lepró, X.; Galvão, D.; Haines, C. Hierarchically buckled sheath-core fibers for superelastic electronics, sensors and muscles. *Science* **2015**, *349*, 400–404. [CrossRef] [PubMed]
77. Leigh, S.J.; Bradley, R.J.; Purssell, C.P.; Billson, D.R.; Hutchins, D.A. A simple, low-cost conductive composite material for 3d printing of electronic sensors. *PLoS ONE* **2012**, *7*, e49365. [CrossRef] [PubMed]
78. Lewis, F.L.; Dawson, D.M.; Abdallah, C.T. *Robot Manipulator Control: Theory and Practice*; Taylor & Francis: Boca Raton, FL, USA, 2003.
79. Kanniah, J.; Ercan, F.; Calderon, C.A.A. *Practical Robot Design: Game Playing Robots*; Taylor & Francis: Boca Raton, FL, USA, 2013.
80. Tadesse, Y.; Thayer, N.; Priya, S. Tailoring the response time of shape memory alloy wires through active cooling and pre-stress. *J. Intell. Mater. Syst. Struct.* **2009**, *21*, 19–40. [CrossRef]
81. Tadesse, Y.; Villanueva, A.; Haines, C.; Novitski, D.; Baughman, R.; Priya, S. Hydrogen-fuel-powered bell segments of biomimetic jellyfish. *Smart Mater. Struct.* **2012**, *21*, 045013. [CrossRef]
82. Joh, H.I.; Ha, T.J.; Hwang, S.Y.; Kim, J.H.; Chae, S.H.; Cho, J.H.; Prabhuram, J.; Kim, S.K.; Lim, T.H.; Cho, B.K. A direct methanol fuel cell system to power a humanoid robot. *J. Power Sources* **2010**, *195*, 293–298. [CrossRef]
83. Maeno, T.; Hino, T. Miniature five-fingered robot hand driven by shape memory alloy actuators. In Proceedings of the 12th IASTED International Conference on Robotics and Applications, Honolulu, HI, USA, 14–16 August 2006; pp. 174–179.
84. Rodrigue, H.; Wei, W.; Bhandari, B.; Ahn, S.H. Fabrication of wrist-like sma-based actuator by double smart soft composite casting. *Smart Mater. Struct.* **2015**, *24*, 125003. [CrossRef]
85. Majima, S.; Kodama, K.; Hasegawa, T. Modeling of shape memory alloy actuator and tracking control system with the model. *IEEE Trans. Control Syst. Technol.* **2001**, *9*, 54–59. [CrossRef]
86. Ma, N.; Song, G.; Lee, H. Position control of shape memory alloy actuators with internal electrical resistance feedback using neural networks. *Smart Mater. Struct.* **2004**, *13*, 777. [CrossRef]
87. Grant, D.; Hayward, V. Variable structure control of shape memory alloy actuators. *IEEE Control Syst.* **1997**, *17*, 80–88. [CrossRef]
88. Elahinia, M.H.; Ashrafiuon, H. Nonlinear control of a shape memory alloy actuated manipulator. *J. Vib. Acoust.* **2002**, *124*, 566–575. [CrossRef]
89. Song, G.; Chaudhry, V.; Batur, C. Precision tracking control of shape memory alloy actuators using neural networks and a sliding-mode based robust controller. *Smart Mater. Struct.* **2003**, *12*, 223–231. [CrossRef]
90. Spong, M.W.; Hutchinson, S.; Vidyasagar, M. *Robot Modeling and Control*; Wiley: New York, NY, USA, 2006; Volume 3.

91. Tadesse, Y.; Priya, S. Graphical facial expression analysis and design method: An approach to determine humanoid skin deformation. *J. Mech. Robot.* **2012**, *4*, 021010. [CrossRef]
92. Dahl, T.S.; Boulos, M.N.K. Robots in health and social care: A complementary technology to home care and telehealthcare? *Robotics* **2013**, *3*, 1–21. [CrossRef]